Sensors and Actuators B 140 (2009) 319–336

Contents lists available at ScienceDirect

Sensors and Actuators B: Chemical

journal homepage: www.elsevier.com/locate/snb

Review

Gas sensors using hierarchical and hollow oxide nanostructures: Overview

Jong-Heun Lee*

Department of Materials Science and Engineering, Korea University, Anam-Dong, Sungbuk-Gu, Seoul 136-713, Republic of Korea

ARTICLE INFO

Article history:
Received 2 March 2009
Received in revised form 6 April 2009
Accepted 13 April 2009
Available online 3 May 2009

Keywords:
Hierarchical nanostructures
Hollow structures
Oxide semiconductor gas sensors
Gas response
Gas response kinetics

ABSTRACT

Hierarchical and hollow oxide nanostructures are very promising gas sensor materials due to their high surface area and well-aligned nanoporous structures with a less agglomerated configurations. Various synthetic strategies to prepare such hierarchical and hollow structures for gas sensor applications are reviewed and the principle parameters and mechanisms to enhance the gas sensing characteristics are investigated. The literature data clearly show that hierarchical and hollow nanostructures increase both the gas response and response speed simultaneously and substantially. This can be explained by the rapid and effective gas diffusion toward the entire sensing surfaces via the porous structures. Finally, the impact of highly sensitive and fast responding gas sensors using hierarchical and hollow nanostructures on future research directions is discussed.

Contents

* Tel.: +82 2 3290 3282; fax: +82 2 928 3584.
E-mail address: jongheun@korea.ac.kr.

0925-4005/$ – see front matter © 2009 Elsevier B.V. All rights reserved.
doi:10.1016/j.snb.2009.04.026

1. Introduction

Oxide semiconductor gas sensors such as SnO_2, ZnO, In_2O_3, and WO_3 show a significant resistance change upon exposure to a trace concentration of reducing or oxidizing gases. At 200–400 °C, an electron depletion layer can be formed near the surface of n-type semiconductors due to the oxygen adsorption with negative charge, which establishes the core (semiconducting)–shell (resistive) structure and the potential barrier between the particles [1–4]. If reducing gases such as CO or H_2 are present in the atmosphere, they are oxidized to CO_2 or H_2O, respectively, by the reaction with negatively charged oxygen and the remnant electrons decrease the sensor resistance. In order to enhance the gas sensitivity, nanostructures with high surface area and full electron depletion are advantageous [5]. In this respect, various oxide nanostructures have been explored, including nanoparticles (0D) [6], nanowires (1D) [7–17], nanotubes (1D) [18–20], nanobelts (quasi 1D) [21,22], nanosheets (2D) [23], and nanocubes (3D) [24].

It has been shown that the gas response increases abruptly when the particle size becomes comparable or smaller than the Debye length (typically several nm) [25]. The uniform dispersion of nanoparticles can be accomplished in a liquid medium via electrostatic and steric stabilization. However, when the nanoparticles are consolidated into sensing materials, the aggregation between the nanoparticles becomes very strong [26,27] because the van der Waals attraction is inversely proportional to the particle size. When the aggregates are large and dense, only the primary particles near the surface region of the secondary particles contribute to the gas sensing reaction and the inner part remains inactive [28]. Under this configuration, a high gas response cannot be achieved because the conductivity change occurs only near the surface region. Moreover, the sluggish gas diffusion through the aggregated nanostructures slows the gas response speed [28].

The 1D nanostructures such as nanowires, nanorods, and nanotubes with a less agglomerated configuration have been used to improve gas sensing characteristics [29,30]. With the recent progress of synthetic routes [31], the improvement of gas sensing characteristics by using 1D SnO_2, In_2O_3, and WO_3 nanostructures has been intensively investigated. In particular, Comini et al. [29] and Kolmakov and Moskovits [30] compiled comprehensive reviews on the potential of quasi 1D metal oxide semiconductors as gas sensors.

Mesoporous oxide structures with well-aligned pore structures [32–34] are another attractive platform for gas sensing reactions [35–37]. The mesoporous structures have been reported to show very high gas responses [38–44] and rapid gas responding kinetics [45], which are attributed to their high surface area and well-defined porous architecture, respectively. The gas response and response speed of mesoporous sensing materials can be improved further by surface modification [39] and doping of catalytic materials [46,47].

Hierarchical nanostructures are the higher dimensional structures that are assembled from low dimensional, nano-building blocks such as 0D nanoparticles, 1D nanowires, nanorods, and nanotubes, and 2D nanosheets. Hierarchical nanostructures show well-aligned porous structures without scarifying high surface area, whereas the non-agglomerated form of oxide nanoparticles is extremely difficult to accomplish. Hollow nanostructures with thin shell layers are also very attractive to achieve high surface area with a less agglomerated configuration. Thus, both a high gas response and a fast response speed can be accomplished simultaneously by using well-designed, hierarchical and hollow oxide nanostructures as gas sensor materials. However, to the author's best knowledge, no review has yet been published that focus on gas sensors using hierarchical and hollow oxide nanostructures. In this paper, synthetic routes and gas sensing characteristics of various hierarchical and hollow oxide nanostructures for application as gas sensors were reviewed. In order to concentrate on gas sensing, the polymeric and non-gas sensing, hierarchical and hollow structures were not included. This review places a special focus on understanding (1) the preparation of hierarchical/hollow oxide nanostructures, (2) the principal parameters to determine the gas sensing reaction, and (3) the mechanism for enhancing the gas sensing characteristics.

2. Definition of hierarchical and hollow structures

A 'hierarchical structure' means the higher dimension of a micro- or nanostructure composed of many, low dimensional, nano-building blocks. The various hierarchical structures were classified according to the dimensions of nano-building blocks and the consequent hierarchical structures, referring to the dimensions, respectively, of the nano-building blocks and of the assembled hierarchical structures (Fig. 1). For example, '1-3 urchin' means that 1D nanowires/nanorods are assembled into a 3D urchin-like spherical shape and '2-3 flower' indicates a the 3D flower-like hierarchical structure that is assembled from many 2D nanosheets. Under this framework, the hollow spheres can be regarded as the assembly of 1D nanoparticles into the 3D hollow spherical shape. Thus, strictly speaking, the 0-3 hollow spheres should be regarded as one type of the hierarchical structures. From now on, for simplicity, the various hollow and hierarchical structures will be referred according to the nomenclature defined in Fig. 1. The 1-3 hollow urchin and 2-3 hollow flower structures shown in Fig. 1 are treated in the section of hollow nanostructures.

3. Strategy to prepare hollow structures for gas sensors

Hollow oxide structures have a variety of applications in the fields of drug delivery, catalysts, energy storage, low dielectric constant materials and piezoelectric materials [48–51]. Lou et al. [52] reported a comprehensive review on the synthesis and applications of hollow micro- and nanostructures. Thus, the main focus of the present review was placed on the synthetic strategies to prepare hollow oxide structures for enhancing the gas sensing characteristics. For gas sensor applications, thin and permeable shell layers are advantageous for complete electron depletion and effective gas diffusion, respectively. Thus far, representative gas sensing materials such as SnO_2, ZnO, WO_3, In_2O_3, α-Fe_2O_3, CuO, and CuS have been prepared as hollow structures. The synthetic routes and morphologies presented in the literature are summarized in Table 1 [53–95]. The chemical routes to prepare hollow oxide structures

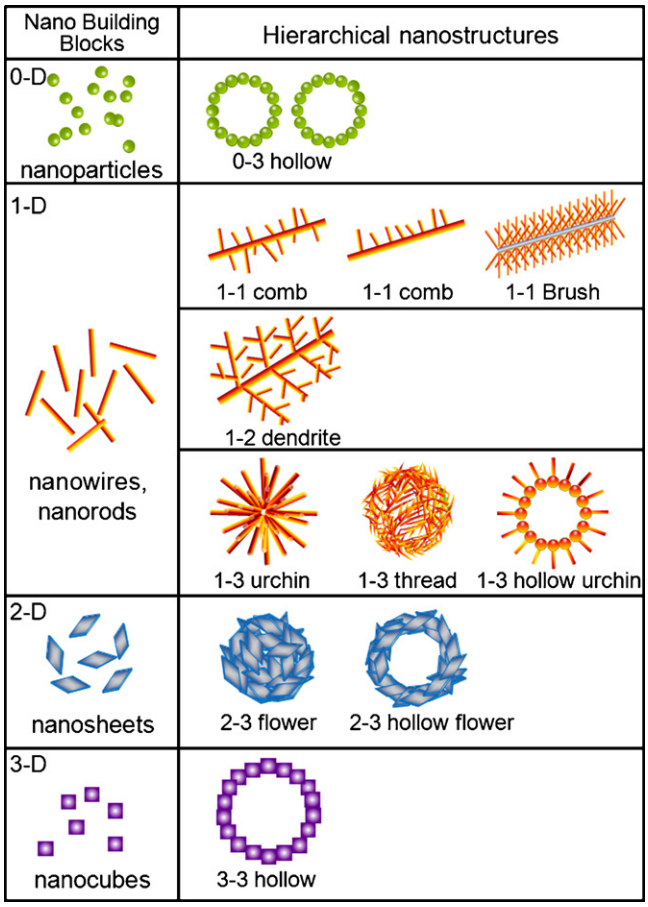

Fig. 1. Nomenclature of hierarchical structures according to the dimensions of the nano-building blocks (the former number) and of the consequent hierarchical structures (the latter number).

are classified into two categories according to the use or not of core templates.

3.1. Preparation of hollow structures using templates

3.1.1. Layer-by-layer (LbL) coating

Hollow oxide spheres can be prepared by the successive, layer-by-layer (LbL) coating of oppositely charged polyelectrolytes and inorganic precursors, followed by the subsequent removal of the template cores (Fig. 2(a)). Metal and polymer spheres, which are used as the sacrificial templates, can be eliminated by dissolution in acidic solution and thermal decomposition, respectively, after the encapsulation procedure. The main advantage is the uniform and precise control of wall thickness of hollow capsules. Caruso et al. [77] prepared TiO_2 hollow microspheres (shell thickness: 25–50 nm) by repetitive coating of positively charged poly(diallyldimethylammonium chloride) (PDADMAC) and negatively charged titanium bis(ammonium lactato) dihydroxide (TALH) on the negatively charged polystyrene (PS) spheres and subsequent removal of the PS templates by heat treatment at 500 °C. They reported that the thickness of the coating layer was increased by approximately 5 nm by increasing the number of TALH/PDADMAC layers deposited. This indicates that the shell thickness of the hollow spheres can be tuned down to 5 nm scale. Caruso et al. [87] also prepared Fe_3O_4 hollow spheres using the LbL method.

3.1.2. Heterocoagulation and controlled hydrolysis

The electrostatic attraction between charged core templates and oppositely charged, fine colloidal particles is the driving force for the coating by heterocoagulation (Fig. 2(b)). The similarity between the LbL process and heterocoagulation is the encapsulation of inorganic layers based on electrostatic self-assembly and the use of sacrificial templates. However, heterocoagulation is a single-step coating procedure, whereas LbL requires multiple-step processes for encapsulation. The short coating time is the main advantage of heterocoagulation. The coating thickness can be manipulated by controlling the concentration of the coating precursor and the diameter, i.e., the surface area of the template spheres [96]. The surface charges of the core templates and coating colloidal particles should be designed very carefully to achieve rapid, reproducible and uniform coating. Kawahashi and Matijević [96] suggested that the anionic and cationic PS templates be chosen according to the charge of colloidal particles for coating. When the hydroxide form of nanoparticles in aqueous solution are coated on the charged PS microspheres, positively charged nanoparticles at pH < isoelectric point (IEP) are necessary to coat the anionic PS while negatively charged nanoparticles at pH > IEP are desirable to coat the cationic PS. Radice et al. [97] prepared PS templates with a positive surface charge by adding NH_3 and PDADMAC and then coating negatively charged TiO_2 nanoparticles by heterocoagulation. Li et al. [78] prepared TiO_2 hollow microspheres by coating negatively charged TiO_2 particles on the positive charge of PS functionalized with cetyltrimethyl ammonium bromide and the core removal. The above shows that the surface charge of PS templates for heterocoagulation can be manipulated in the preparation stage or by functionalizing the surface using charged polyelectrolytes.

The controlled hydrolysis reaction can be defined as the gradual encapsulation of hydroxide by heterogeneous nucleation on the neutral or very-weakly charged templates (Fig. 2(c)). For this, the kinetics of the hydrolysis reaction should be slow because rapid hydrolysis usually leads to the precipitation of separate particles. The present author and co-workers coated a Ti-hydroxide layer on Ni spheres by the gradual hydrolysis reaction of the $TiCl_4$ butanol solution containing diethylamine (DEA) and a trace concentration of water [79,80]. The reaction between DEA and a small amount of water gradually provided OH^- ions for the slow hydrolysis reaction and Ti-hydroxide was uniformly coated on the surface of spherical Ni template.

Strictly speaking, the surface charges of nanoparticles or templates, even if they are very weak, cannot be excluded completely. Thus, heterocoagulation after gradual precipitation via controlled hydrolysis reaction is a feasible and promising route. Shiho and Kawahashi [86] prepared Fe_3O_4 hollow spheres by this approach. It should be noted that pH is a critical parameter not only to control the hydrolysis reaction but also to determine the surface potential of metal hydroxide nanoparticles in aqueous solution.

3.2. Preparation of hollow structures without templates

3.2.1. Hydrothermal/solvothermal self-assembly reaction

Hydrothermal/solvothermal reaction offers a chemical route to prepare well-defined oxide nanostructures [98–101]. The Teflon-lined autoclave provides a high pressure for the accelerated chemical reaction at relatively low temperature (100–250 °C), which make it possible to prepare highly crystalline oxide nanostructures. The hollow precursor or oxide particles can be prepared either by the chemically induced, self-assembly of surfactants into micelle configuration or by the polymerization of carbon spheres and subsequent encapsulation of metal hydroxide during the hydrothermal/solvothermal reaction (Fig. 3(a)). Zhao et al. [59] prepared SnO_2 hollow spheres from a micelle system that is made up of the surfactants terephtalic acid and sodium dodecyl benzenesulfonate (SDBS) in ethanol and water. Yang et al. [58] fabricated multilayered SnO_2 hollow microspheres by preparing multilayered SnO_2–carbon composites via the hydrothermal self-assembly reac-

Table 1
The morphologies and synthetic routes of various hollow oxide structures presented in the literature for gas sensor applications [53–95].

Material	Hierarchy and morphology		Preparation	Reference
SnO_2	0-3	Hollow	Sol–gel using PMMA, PS, carbon templates	[53,54,55]
			Sol–gel using crystalline array of PS	[56]
			LbL deposition using PS template	[57]
			Hydrothermal/solvothermal self-assembly	[59,59]
			Hydrothermal	[60]
			Hydrothermal Ostwald ripening	[61,62]
			Ultrasonic spray pyrolysis	[63]
ZnO	0-3	Hollow	Hot solution self-assembly	[64]
			Hydrothermal/solvothermal self-assembly	[65,66]
			Sol–gel using carbon templates	[67]
			Hydrothermal Ostwald ripening	[68]
	1-3	Hollow urchin	Hydrothermal/solvothermal self-assembly	[69,70]
			Precursor-templated thermal evaporation	[71]
	2-3	Hollow flower	Hydrothermal/solvothermal self-assembly	[69,72]
WO_3	0-3	Hollow	Controlled hydrolysis using carbon template	[73]
			Hydrothermal self-assembly	[74]
	2-3	Hollow flower	Heat treatment of acid-treated $SrWO_4$	[75]
TiO_2	0-3	Hollow	Sol–gel using crystalline array of PS	[56]
			LbL deposition using PS template	[77]
			CTAB-mediated heterocoagulation using PS template	[78]
			Controlled hydrolysis using Ni template	[79,80]
			Ultrasonic spray pyrolysis	[81]
			Hydrothermal Ostwald ripening	[82]
	0-3	Hemi-hollow[a]	Sputtering on PMMA template	[83]
In_2O_3	0-3	Hollow	Solvothermal self-assembly	[84]
	3-3	Hollow	Vesicle template interface route	[85]
Fe_3O_4/α-Fe_2O_3	0-3	Hollow	Controlled hydrolysis and heterocoagulation using PS template	[86]
		Hollow	LbL deposition using template	[87]
		Hollow	Solvothermal Ostwald ripening	[88]
	1-3	Hollow urchin	Controlled hydrolysis on the polyelectrolyte- multilayer-coated particles	[89]
Cu_2O/CuO	0-3	Hollow	Solvothermal self-assembly	[90,91]
	2-3	Hollow flower	Biomolecule-assisted hydrothermal self-assembly	[92]
NiO	2-3	Hollow flower	Controlled hydrolysis using PSA template	[93]
CuS	0-3	Hollow	Surfactant micelle-template inducing reaction	[94]
ZnO–SnO_2	0-3	Hollow	Hydrothermal self-assembly	[95]

[a] Hemispherical hollow.

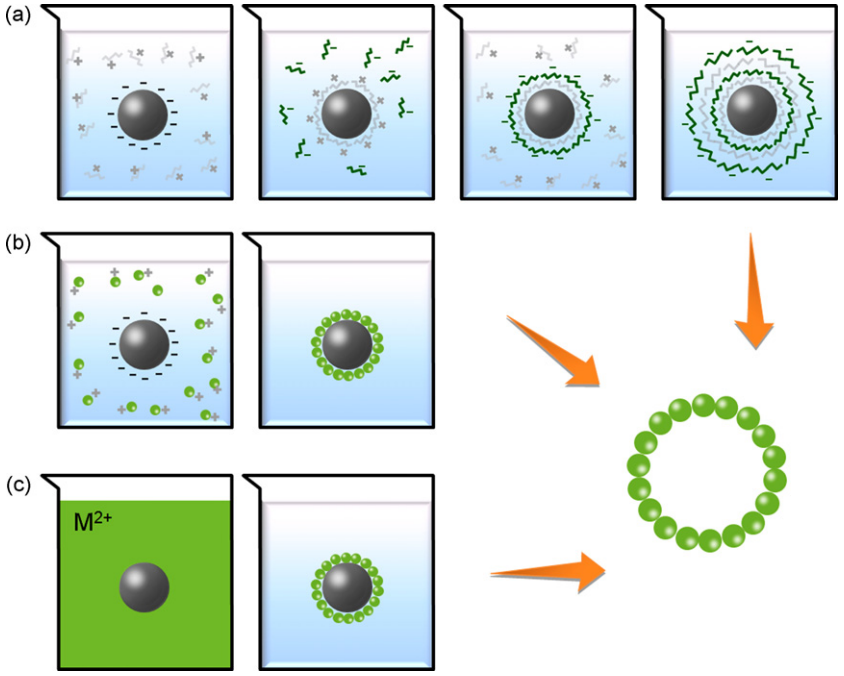

Fig. 2. Schematic diagrams for the preparation of hollow structures using the (a) layer-by-layer (LbL) coating method, (b) heterocoagulation and (c) controlled hydrolysis.

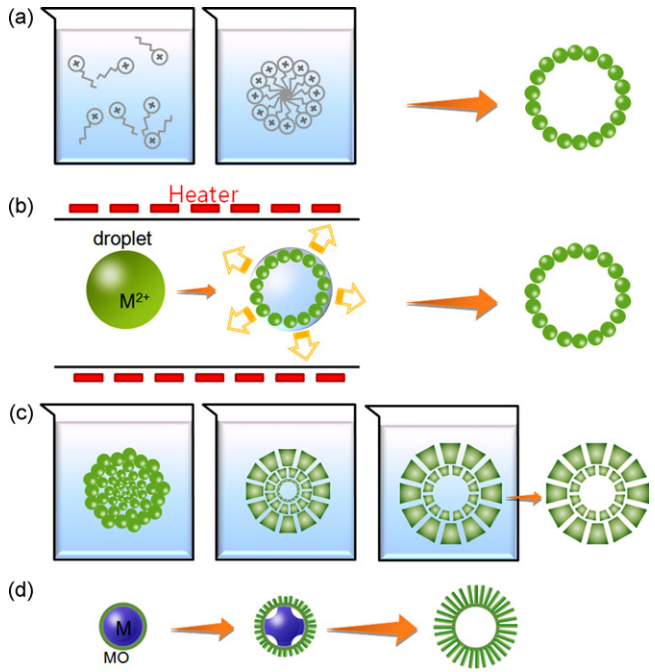

Fig. 3. Schematic diagrams for the preparation of hollow structures using the (a) self-assembled hydrothermal/solvothermal reaction, (b) spray pyrolysis, (c) Ostwald ripening of porous secondary particles, and (d) solid evacuation by the Kirkendall effect.

tion of aqueous sucrose/$SnCl_4$ solution and subsequent removal of carbon components. Usually, the core polymer parts are removed by heat treatment at elevated temperature (500–600 °C). Thus, hollow oxide structures can be used stably as gas detection materials at the sensing temperature of 200–400 °C without thermal degradation.

3.2.2. Spray pyrolysis

Spray pyrolysis is a synthetic route to prepare spherical oxide particles by the pyrolysis of small droplets containing cations at high temperature. Nozzle and ultrasonic transduction are used to produce aerosols in the order of several micrometers (Fig. 3(b)). If the solvent evaporates rapidly or the solubility of the source materials is low, local precipitation occurs near the droplet surface, which leads to the formation of hollow spheres [102–104]. In order to prepare hollow spheres by spray pyrolysis, droplets with a short retention time at high temperature are desirable to attain the high supersaturation at the droplet surface prior to the evaporation of the entire solvent. Usually, no templates are necessary to produce hollow structures in spray pyrolysis. Moreover, multicompositional powders with uniform composition can be prepared easily because each droplet plays the role of a reaction container [105–108]. However, the reproducible tuning of shell thickness requires comprehensive understanding of the solvent evaporation, the solubility of the source materials and pyrolysis of the precursor during the entire spray pyrolysis reaction. Because each droplet is converted into the oxide sphere separately at high pyrolysis temperature, the powders after drying can be redispersed in a liquid medium for processing into sensors. SnO_2 and TiO_2 [81] hollow spheres have been prepared by ultrasonic spray pyrolysis.

3.2.3. Ostwald ripening of porous secondary particles

Ostwald ripening is a coarsening of crystals at the expense of small particles. The hollow structures can be formed via Ostwald ripening at the secondary microspheres containing nano-size primary particles. If the primary particles in the outer part of the microspheres are larger or packed in a denser manner than those in the inner part, they grow at the expense of those in the core. This Ostwald ripening gradually transforms the porous microspheres into hollow ones (Fig. 3(c)). It is supported by the observation that the coarsened particles at the shell layer show cellular morphology and are highly organized with respect to a common center [82,88]. The key factors in the design of hollow structures via Ostwald ripening were reviewed by Zeng [109]. The primary particles should be packed in a loose manner for effective dissolution during the hydrothermal/solvothermal reaction. Lou et al. [61] prepared hollow SnO_2 spheres (size: ~200 nm) and suggested solid evacuation by Ostwald ripening as the hollowing mechanism. The preparation of extremely thin hollow spheres is difficult because the shell thickness is primarily determined by the initial packing density of the primary particles and the particle size difference between the shell and core layers.

3.2.4. The Kirkendall effect

During the oxidation of dense and crystalline metal particles, hollow structures can be developed by the Kirkendall effect when the outward diffusion of metal cations through the oxide shell layers is very rapid compared to the inward diffusion of oxygen to the metal core [110–112] (Fig. 3(d)). Solid evacuation is the common aspect of Ostwald ripening and the Kirkendall effect. However, in principle, the shell layers developed by the Kirkendall effect are denser and less permeable than those by Ostwald ripening. Gaiduk et al. [113] changed the heat treatment temperatures and the oxygen partial pressures during the oxidation of 50–100 nm Sn particles and found that the hollowing process is enhanced by increasing the heat treatment temperature or oxygen concentration. This reflects the formation of SnO_2 hollow spheres via the Kirkendall effect. However, they also pointed out that the adsorption of oxygen with the negative charge, which is well known in gas sensing mechanism, can promote the outward migration of metal ions by developing an electric field.

4. Gas sensors using hollow oxide structures

4.1. Principal parameters to determine gas sensing characteristics

4.1.1. Shell thickness

The key parameters to determine the gas sensing characteristics of hollow oxide structures are the thickness, permeability, and surface morphology of the shell layer. When the shells are very dense and thick, the gas sensing reaction occurs only near the surface region of hollow spheres (Fig. 4(a)), while the inner part of the hol-

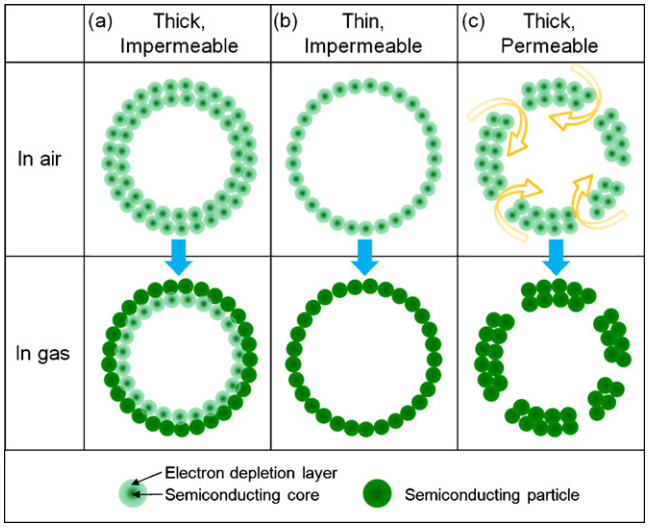

Fig. 4. Key parameters to determine the gas responses in hollow structures.

low spheres become inactive. However, if the shell is sufficiently thin, the entire primary particles in hollow spheres become active in gas sensing reaction, even when the shells are less permeable (Fig. 4(b)). In addition, the gas response speed of hollow spheres increases at the thinner shell configuration due to the rapid gas diffusion. This is analogous to enhancing the gas response [114–116] and/or gas responding kinetics [117] by decreasing the film thickness in the thin-film gas sensors.

The main approaches to tune the shell thickness are (1) increasing the coating procedures during the LbL process, (2) manipulating the concentration of source solution during heterocoagulation and controlled hydrolysis reactions, and (3) controlling the local precipitation at the surface region of the droplets by manipulating the solubility of source materials or the rate of solvent evaporation during spray pyrolysis reaction.

4.1.2. Shell permeability

When the shell layers are nano- or microporous, the target gases for detection and the oxygen for the recovery can diffuse to both the inner and surface regions of hollow spheres (Fig. 4(c)). Thus, a high gas response can be accomplished even with relatively thick shell layers so long as the gas diffusion through the pores of hollow spheres is not hampered significantly. The three approaches to achieve the gas-permeable porous shells are described below.

- Abrupt decomposition of the core polymer: the polymer or carbon templates are used in the LbL method, heterocoagulation, controlled hydrolysis, and hydrothermal reaction in order to prepare hollow oxide structures. If the core templates are decomposed gradually by slow heating, the hollow structures of the oxide shell can be preserved. In contrast, the rapid thermal decomposition of core templates produces many nano- and mesopores on the surface of hollow oxide spheres and cracks the hollow structures [118]. Kawahashi and Matijević [118] prepared yttrium–carbonate-encapsulated PS spheres and removed the PS by thermal decomposition. Complete shells were obtained from calcination at a heating rate of 10 °C/min, whereas cracked hollow particles were observed from calcination at a heating rate of 50 °C/min.
- Ballooning of the core template: the ballooning effect due to the increased volume of the core templates can induce porosity of the shell layer. The present author and co-workers encapsulated Ti-hydroxide layers on Ni spheres via controlled hydrolysis reaction [79]. The Ti-hydroxide-encapsulated Ni particles were immersed in dilute HCl for a week but the dissolution of metal cores was impossible. After heat treatment at 400 °C for 1 h, however, the core Ni could be removed by dilute HCl solution (Fig. 5(a)). The present author and co-workers prepared the SnO_2 hollow spheres by encapsulating the Sn-precursor on Ni spheres and then removing the metal templates (Fig. 5(b)) [119]. The Ni cores could be removed by dilute HCl only after heat treatment at 400 °C for 1 h. These findings were attributed to the change of shell structure into a porous one by the ballooning of cores due to the volume increase during the oxidation of Ni.
- Evaporation of solvent or decomposition of precursor during spray pyrolysis: During the spray pyrolysis reaction, if local precipitation occurred in the outer parts of the droplets, the remaining solvent in the inner part evaporates through the shell layer. If the precipitate shell is highly permeable and plastic, the hollow morphology can be preserved even after the solvent evaporation or precursor decomposition. However, when the precipitate shells are impermeable and rigid, high pressure will be developed due to the vapors formed by solvent evaporation or precursor decomposition, which eventually produces many pinholes at the hollow spheres or cracks the hollow spheres [102]. On the other hand, the porosity of spherical powders can be increased by adding a polymer precursor to the source solution in spray pyrolysis. For example, Hieda et al. [120] prepared macroporous SnO_2 spheres by ultrasonic spray pyrolysis of the source solution containing polymethylmethacrylate (PMMA) microspheres.

4.1.3. Surface morphology of the shell

The 0-3 hollow shells usually have a smooth surface. In this condition, the primary parameters to determine the gas response are the thinness and permeability of shells. In contrast, the 1-3 hollow urchin-like and 2-3 hollow flower-like hierarchical structures can provide a higher surface area, which further enhances the gas response. The present author and co-workers grew SnO_2 nanowires on SnO_2 hollow spheres (prepared by Ni templates) via vapor phase growth after the coating of the Au catalyst layer [119]. Fig. 6 shows the scanning electron micrograph of 1-3 SnO_2 hollow urchin structures. The enhancement of gas response induced by using urchin-like hollow morphologies will be treated in the following section.

4.2. Gas sensing characteristics of hollow oxide structures

Martinez et al. [57] prepared Sb-doped SnO_2 hollow spheres by LbL coating on PS templates and fabricated the gas sensors on MEMS structures. The R_a/R_g ratios of Sb:SnO_2 hollow spheres to 0.4–1 ppm CH_3OH at 400 °C were approximately 3- and 5-fold higher than those of SnO_2 polycrystalline chemical vapor deposition films and Sb:SnO_2 microporous nanoparticle films, respectively (Fig. 7). Zhao et al. [59] prepared SnO_2 hollow spheres by the solvothermal reac-

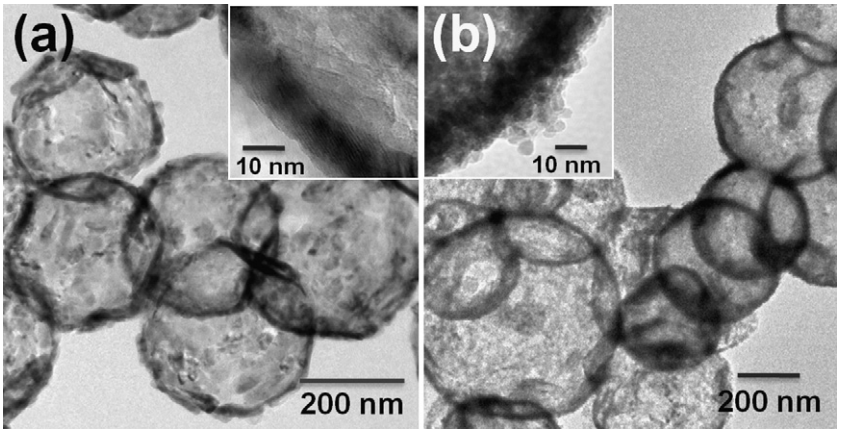

Fig. 5. (a) TiO_2 hollow spheres and (b) SnO_2 hollow spheres prepared by the encapsulation of Ti- and Sn-precursors on Ni spheres and the removal of core metal templates by dilute HCl aqueous solution after heat treatment at 400 °C ((a) according to [79]).

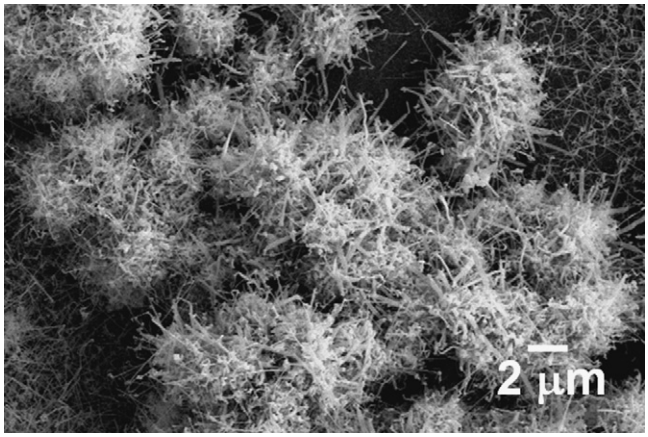

Fig. 6. Scanning electron micrograph of 1-3 urchin-like SnO_2 hollow spheres prepared by vapor phase growth of SnO_2 nanowires on the SnO_2 hollow spheres after coating of Au catalyst layer. The SnO_2 hollow spheres were prepared by encapsulation of a Sn-precursor on the Ni templates and the subsequent removal of the core Ni by dilute HCl aqueous solution.

tion of ethanol/water solution containing SDBS and terephthalic acid. They reported that the R_a/R_g ratio of hollow structures to 50 ppm C_2H_5OH at room temperature is ~5.2-fold higher than that of nanoparticles. Wang [60] also reported a 5.2- to 20-fold enhancement in gas responses to 75–900 ppm C_2H_5OH by using SnO_2 hollow structures. Zhang et al. [55] reported that the SnO_2 hollow spheres prepared by the sol–gel coating of Sn-precursor on carbon templates exhibited a 8.0- to 12.2-fold increase in gas responses to 5–100 ppm NO_2 in comparison to nanoparticles.

Kim et al [83] prepared hemispherical, hollow TiO_2 gas sensors by depositing a TiO_2 thin film onto self-assembled, sacrificial PMMA templates using RF sputtering and subsequently removing the spherical templates via thermal decomposition at 450 °C. The gas response of the hemispherical, hollow TiO_2 thin films to 0.5–5 ppm NO_2 at 300 °C was ~2-fold higher than that of plain (untemplated) TiO_2 thin films. They [121] also reported the enhancement of H_2 response by applying this microsphere templating route to the preparation of $CaCu_3Ti_4O_{12}$ film. These results can be attributed to the decreased film thickness close to the scale of the electron depletion layer and the effective gas diffusion through the macroporous network between the TiO_2 hemispheres with monolayer configuration.

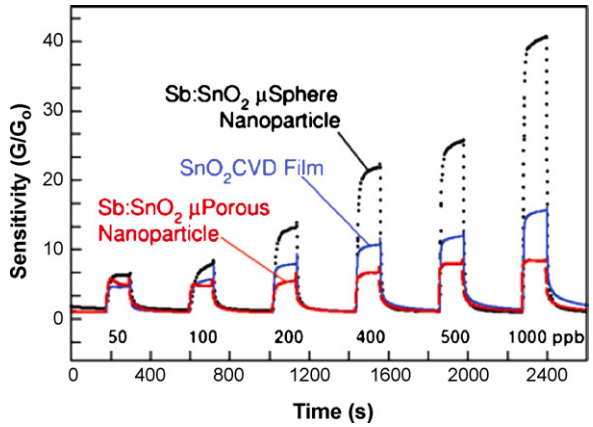

Fig. 7. Sensitivity (to methanol) comparison of a hollow Sb:SnO_2 nanoparticle microspheres film, a SnO_2 chemical vapor deposition film, and an Sb:SnO_2 microporous nanoparticles film. Sensitivity was obtained by dividing the conductance (G) by the baseline conductance (G_0). All films were tested within a single element micro-hot-plate array device. Reproduced with permission from Ref. [57].

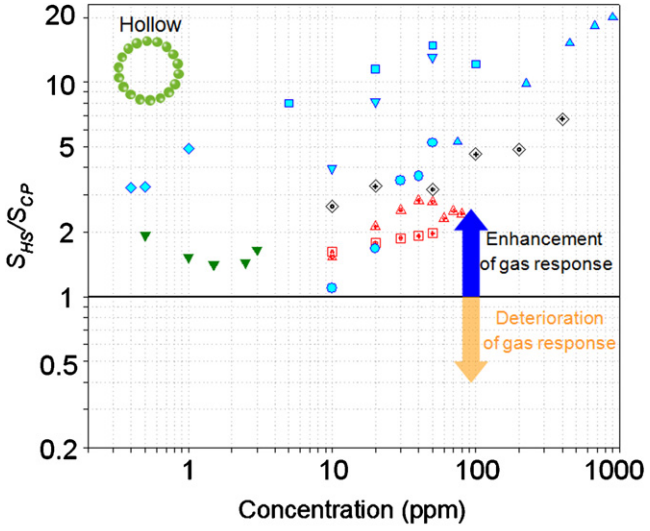

	HS[a)]	Mater.	Gas	T_{sens}(°C)	CP[b)]	Ref.
◆	0-3 Hollow	$Sb:SnO_2$	CH_3OH	400	NP[c)]	[57]
●	0-3 Hollow	SnO_2	C_2H_5OH	r.t.	NP	[59]
▲	0-3 Hollow	SnO_2	C_2H_5OH	r.t.	NP	[60]
▼	0-3 Hollow	SnO_2	C_2H_5OH	290	NP	[62]
■	0-3 Hollow	SnO_2	NO_2	160	NP	[55]
▼	0-3 Hemi-hollow	TiO_2	NO_2	300	Film	[83]
◇	0-3 Hollow	CuS	CH_3COCH_3	210	NP	[94]
⊞	0-3 Hollow	In_2O_3	CO	400	NP	[84]
⊿	3-3 Hollow	In_2O_3	C_2H_5OH	r.t.	NC[d)]	[85]

Fig. 8. Ratios between the gas responses of hollow oxide structures ($S_{HS} = R_a/R_g$ or R_g/R_a of hollow structures) and those of counterparts for comparison ($S_{CP} = R_a/R_g$ or R_g/R_a of counterparts). (a) HS: hollowstructures, (b) CP: counterparts for comparison, hemi-hollow: hemispherical, hollow, (c) NP: nanoparticles and (d) NC: nanocrystalline commercial powders. Note that the gas response in ref. [55] is R_g/R_a. The data in the figure were estimated from Refs. [55,57,59,60,62,83–85,94]..

Choi et al. [89] prepared α-Fe_2O_3 hollow urchin spheres by the formation of the FeOOH crystallites within a polyelectrolyte multilayer (PEM) that was coated on polymer templates and subsequent heat treatment at 700 °C for 12 h. As the reaction time to form the FeOOH–PEM composites increased, the shell became thicker and the nanorods on the surfaces of the hollow urchins lengthened. The gas responses of the thicker hollow spheres to 200–5000 ppm C_2H_5OH were ~3-fold higher than those of the thinner ones. If the shell is impermeable and smooth, the gas response should decrease as the shell becomes thicker. The higher gas responses in the thicker shells in this paper was attributed to the enhanced surface area due to the thornier configuration of surface, possibly in combination with the permeable shell.

The gas sensing characteristics of hollow oxide structures in the literature were compiled and the results are summarized in Fig. 8. In general, the R_a/R_g (or R_g/R_g) ratios upon exposure to a fixed concentration of gas should be identical at a constant sensing temperature, regardless of the variation of the gas sensing apparatuses. However, in this overview, for the more precise and reliable comparison, we used only the literature data containing the R_a/R_g (or R_g/R_g) ratios of both hollow structures (denoted as S_{HS}) and counterparts for comparison (denoted as S_{CP}). A S_{HS}/S_{CP} ratio > 1 indicates an improved gas response and $S_{HS}/S_{CP} < 1$ does a deteriorated gas response by using hollow oxide structures. As can be seen in Fig. 8, all the S_{HS}/S_{CP} ratios are higher than unity, indicating that hollow microspheres are advantageous to enhance the gas response.

The present author and co-workers prepared In_2O_3 hollow microspheres by solvothermal self-assembly reaction and measured the gas sensing characteristics (Fig. 9) [84]. The gas responses

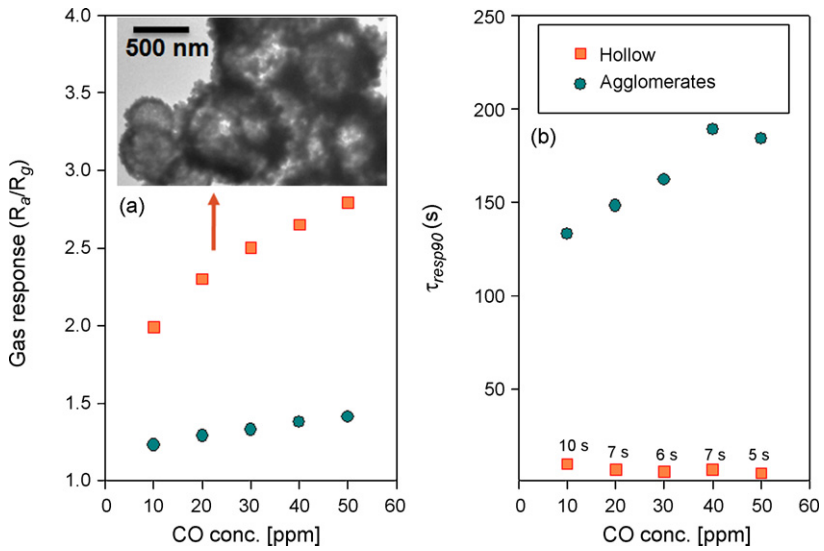

Fig. 9. (a) Gas response (R_a/R_g) to 10–50 ppm CO, and (b) 90% response time (τ_{resp90}) of the hollow In_2O_3 microspheres and In_2O_3 nanoparticles at 400 °C, according to Ref. [84].

Table 2
Response times of hollow oxide structures in the literature [54,84,89,91,94].

Materials	Hierarchy and morphology	Gas and concentration	T_{sens} (°C)[a]	Response time (s)	Reference
SnO_2	0-3 Hollow	100 ppm C_2H_5OH	300	4	[54]
In_2O_3	0-3 Hollow	10–50 ppm CO	400	<10 s	[84]
α-Fe_2O_3	1-3 Hollow urchin	200–5000 ppm C_2H_5OH	300	20 s	[89]
Cu_2O/CuO	0-3 Hollow	400 ppm CO	320	<10 s	[91]
Cu_2O/CuO	0-3 Hollow	2 ppm C_2H_5OH	320	<10 s	[91]
CuS	0-3 Hollow	20–800 ppm C_2H_5OH	210	~15 s	[94]

[a] Sensing temperature.

of In_2O_3 hollow microspheres to 10–50 ppm CO were 1.6–2-fold higher than those of In_2O_3 nanoparticles (Fig. 9(a)). Moreover, the gas response speed was 13- to 37-fold increased by using hollow structures (Fig. 9(b)). The high gas response and rapid response kinetics were explained by the effective and rapid gas diffusion toward the entire sensing surface via the thin and permeable shell layers.

The above results clearly reveal the very fast response speed and high gas response that can be achieved by the use of hollow oxide structures. There is a paucity of data in the literature showing the response times of both hollow structures and counterparts for comparison. Thus, the representative response times of only hollow spheres are summarized in Table 2 [54,84,89,91,94]. The response times upon exposure to gas ranged from 4 to 15 s. The typical gas response times for oxide semiconductor-type gas sensors are in the range of 30–300 s [122–124] although the responding kinetics are also dependent on the sensing temperature. The very short response time of hollow oxide structure should be understood in the framework of rapid gas diffusion to the sensing surface due to the thin and/or nanoporous shell structures. This clearly confirms that the hollow oxide structures are very promising for highly sensitive and fast responding gas sensor materials.

5. Strategy to prepare hierarchical nanostructures for gas sensors

The periodically assembled, hierarchical oxide structures provide a high surface area for chemical reaction, effective diffusion of chemical species (ions or gases) into the interface/surface, and enhanced light scattering [125]. The main applications of hierarchical structures, therefore, are the removal of heavy metal ions [126], gas sensors [127], photocatalysts [128–130], dye-sensitized solar cells [125], and electrode materials for batteries [131]. The van der Waals attraction between hierarchical structures is relatively weak because the hierarchical structures are generally larger than the individual nanostructures. And the hierarchically assembled microspheres are more flowable than the anisotropic shapes of nanostructures such as nanowires and nanosheets. Accordingly, the hierarchically assembled microspheres are advantageous in dispersion, slurry formation, and thick-film formation. The literature data on the preparation of hierarchical oxide structures for gas sensor applications are summarized in Table 3 [23,60,65,84,132–165]. As stated before, the hollow structures should be included within a wide concept of hierarchical structures. However, in the Sections 5 and 6, the preparation and gas sensing characteristics of hierarchical structures except hollow structures will be considered. The vapor phase growth and hydrothermal/solvothermal reaction are two important synthetic routes for hierarchical oxide nanostructures.

5.1. Vapor phase growth

Vapor phase growth is a representative method to prepare 1D nanostructures such as nanowires and nanorods via the vaporization of source materials and their condensation to form the desired product [166–168]. The mechanisms for 1D growth include the following:

(1) vapor–liquid–solid growth (VLS process using metal catalyst) [169].
(2) oxide-assisted growth (VLS process using a small amount of oxide) [170].
(3) vapor–solid growth (VS process without metal catalyst) [171].

Table 3
The morphologies and synthetic routes of various hierarchical oxide structures for gas sensor applications in the literature [23,60,65,84,132–165].

Material	Hierarchy and morphology		Preparation	Reference
SnO_2	1-1	Brush	Two-step vapor phase growth	[132]
			Vapor phase growth	[133]
	1-3	Urchin	Hydrothermal/solvothermal	[60,134–136]
	2-3	Flower	Hydrazine method	[23]
			Hydrothermal	[136,137]
ZnO	1-1	Comb	Vapor phase growth	[138]
		Brush tube	Hydrothermal Ostwald ripening	[139]
	1-2	Dendrite	Vapor phase growth	[140]
			Hydrothermal	[141]
	1-3	Urchin	Hydrothermal/solvothermal self-assembly	[65]
			Hot solution self-assembly	[142,143]
			Microwave-assisted solution method	[144]
			Vapor phase growth	[145]
	2-3	Flower	Hydrothermal	[146–148]
			Hot solution self-assembly	[143]
WO_3	1-1	Brush	Two-step vapor phase growth	[149]
	1-3	Urchin	Hydrothermal	[150]
	1-3	3D network	Vapor phase growth	[151,152]
TiO_2	2-3	Flower	Agar–gel-based solution growth	[153]
In_2O_3	1-3	Urchin	Hydrothermal self-assembly	[84]
α-Fe_2O_3	1-2	Dendrite	Microwave hydrothermal	[154]
	1-3	Urchin	Microwave-assisted reaction	[155]
	1-3	Hexapod	Hydrothermal	[156]
CuO	1-3	Urchin	Microwave hydrothermal	[157,158]
		Thread ball	Hydrolysis of metal–ammonia complex ion	[159]
	2-3	Flower	Hydrothermal	[158]
NiO	1-3	Urchin	Hydrothermal	[160]
SnO_2/α-Fe_2O_3	1-1	Brush	Hydrothermal next to coordination-assisted dissolution	[161]
			Two-step hydrothermal	[162]
ZnO/SnO_2	1-1	Brush	Two-step vapor phase growth	[132]
ZnO/In_2O_3	1-1	Brush	Two-step vapor phase growth	[163]
ZnO/Ga_2O_3	1-1	Brush	Two-step vapor phase growth	[164]
Ga_2O_3/In_2O_3	1-1	Brush	Vapor phase growth	[165]

(4) carbothermal reaction (formation of a metal suboxide or precursor by the reaction of metal oxide with carbon and its subsequent oxidation into oxide nanowires) [172].

Most of the 1-1 comb-like and 1-1 brush-like hierarchical structures in Table 1 were prepared by two-step, vapor phase growth, i.e., the growth of branch nanowires after the formation of core nanowires. The SnO_2 (branch nanowires)/SnO_2 (core nanobelts) [132] have been prepared by two-step, vapor growth. Baek et al. [149] prepared W/WO_3 hierarchical heteronanostructures by the growth of W nanothorns on the surface of WO_3 whiskers by carbothermal reduction of WO_3. The hydrothermal growth of SnO_2 branch nanowires on α-Fe_2O_3 nanorods [162] for gas sensor application was also reported. The symmetries of 1-1 hierarchical nanobrushes are dependent upon those of core nanowires because the outer secondary nanowires grow perpendicular to the core ones [163,164]. Thus, the growth direction and the number density of the outer secondary nanowires can be manipulated by the facet number and the diameter of the inner core nanowires, respectively.

5.2. Hydrothermal/solvothermal self-assembly reaction

Hydrothermal/solvothermal reaction provides a chemical route to prepare highly crystalline oxides or precursors. Under certain conditions, the crystalline nano-building blocks can be assembled into higher dimensional hierarchical structures. Generally, the formation of small aggregates of nano-building blocks is necessary as the nuclei and subsequent radial growth of single crystalline oxide nanowires/nanorods on the spherical nuclei can lead to an urchin-like morphology. The agglomeration of 1D or 2D nano-building blocks into spherical morphology might be considered as a possible mechanism to construct 1-3 thread-ball-like or 2-3 flower-like hierarchical structures, respectively. Nevertheless, the detailed formation mechanisms for various hierarchical structures during hydrothermal/solvothermal reaction remain unclear.

The 0D, 1D, and 2D nano-building blocks are commonly assembled into hierarchical structures with spherical morphology. The construction of well-aligned hierarchical structures, thus, imparts an isotropic nature. Although the overall dimensions of hierarchical structures during hydrothermal/solvothermal reaction are difficult to control, the dimensions of elementary nano-building blocks can be manipulated. Ohgi et al. [136] prepared various SnO_2 hierarchical structures by aging SnF_2 aqueous solution at 60 °C. The morphology of the assembled hierarchical structures could be manipulated from 0 to 3 spheres via 1-3 pricky (urchin-like) particles to 2-3 aggregates of plates by controlling the SnF_2 concentration, pH, and aging time of the stock solution (Fig. 10). The major phase of the 2-3 aggregates of the nanoplates was SnO and it was converted into SnO_2 by heat treatment at 500 °C for 3 h. The present author and co-workers prepared the assembled hierarchical form of SnO nanosheets by a room temperature reaction between $SnCl_2$, hydrazine, and NaOH [23]. These hierarchical structures could also be oxidized into SnO_2 without morphological change by heat treatment. The SnO nanostructures in the literature show 2D morphologies such as sheet and diskette [173,174], indicating that the 2D morphology emanates from the crystallographic characteristics of SnO. In this regards, the dimensions of nano-building blocks within the hierarchical structure can be designed either by manipulating the processing conditions or by controlling the phase of the precursor or suboxide.

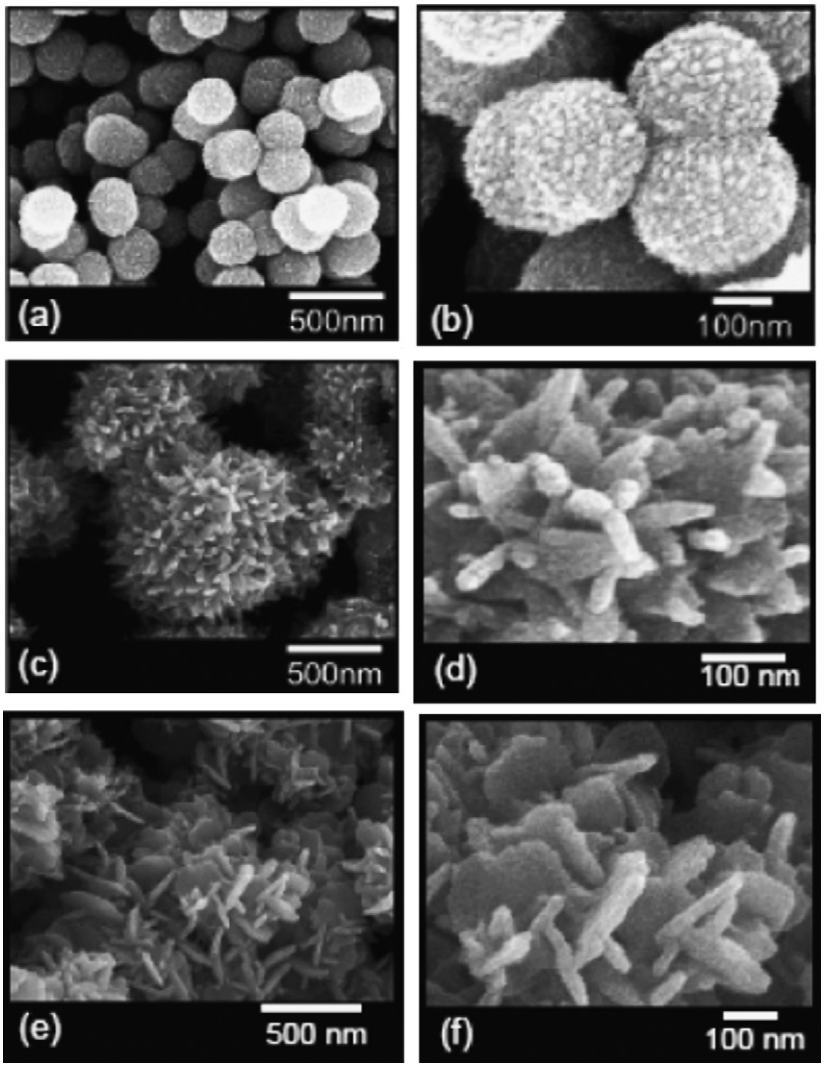

Fig. 10. SEM images of spheres (a and b), pricky particles (c and d), and aggregates of plates (e and f) grown for 24 h at pH 3.20 with 10, 150, and 300 mM of SnF_2 concentration, respectively. Reproduced with permission from Ref. [136].

6. Gas sensors using hierarchical oxide structures

6.1. Principal parameters to determine gas sensing characteristics

6.1.1. Dimensions of nano-building blocks

The surface area for gas sensing in hierarchical structures is determined by the dimensions and packing configuration of nano-building blocks. For example, in 1-1 brush-like hierarchical structures, the area for the growth of branch nanowires is defined by the surface area of the core nanowires. Thus, the growth of thinner branch nanowires with a higher number density will provide a higher surface area for gas sensing reaction.

This principle can also be applied to the 1-3 urchin-like nanostructures (Fig. 11(a) and (b)). If the identical diameter ($d = 2r$) and length (h) of n cylindrically shaped nanowires grow on a spherical nucleus (radius: R) with a constant coverage (Fig. 11(e)), the coverage of nanowires (θ) will be determined by the ratio between the surface area of the core nucleus ($4\pi R^2$) and the total bottom area of the n nanowires ($n\pi r^2$) because the basal area of the nanowires can be approximated by the values calculated from planar ones when the diameter of the nanowires is very small.

$$\theta \cong \frac{n\pi r^2}{4\pi R^2} \tag{1}$$

The specific surface area of an urchin-like microsphere is:

$$S = \frac{n(2\pi rh + \pi r^2) + 4\pi R^2(1-\theta)}{n(\pi r^2 h)\rho + (4/3)\pi R^3 \rho} \tag{2}$$

where ρ is the density of nanowires. Generally, it can be assumed that the surface area of the uncovered part of a core nucleus ($4\pi R^2(1-\theta)$) is negligible compared to the total surface area of n nanowires ($n(2\pi rh + \pi r^2)$) and that the mass of the core nucleus ($4\pi R^3\rho/3$) is much smaller than that of n nanowires ($n(\pi r^2 h)\rho$). Thus, the equation can be reduced to the following in the case of numerous, very thin and long nanowires.

$$S \cong \frac{n(2\pi rh + \pi r^2)}{n(\pi r^2 h)\rho} = \frac{1}{\rho}\left(\frac{2}{r} + \frac{1}{h}\right) \tag{3}$$

Furthermore, '$1/h$' in the equation can also be neglected because the length of the nanowire is much greater than its diameter ($h \gg 2r = d$).

$$S \cong \frac{2}{\rho r} = \frac{4}{\rho d} \tag{4}$$

This equation implies that the surface area of 0-3 urchin-like microspheres is inversely proportional to the nanowire's diameter (d) (Fig. 11(a) and (b)). Thus, the thinner thorns in the 1-3 urchin-like hierarchical structures are advantageous in improving

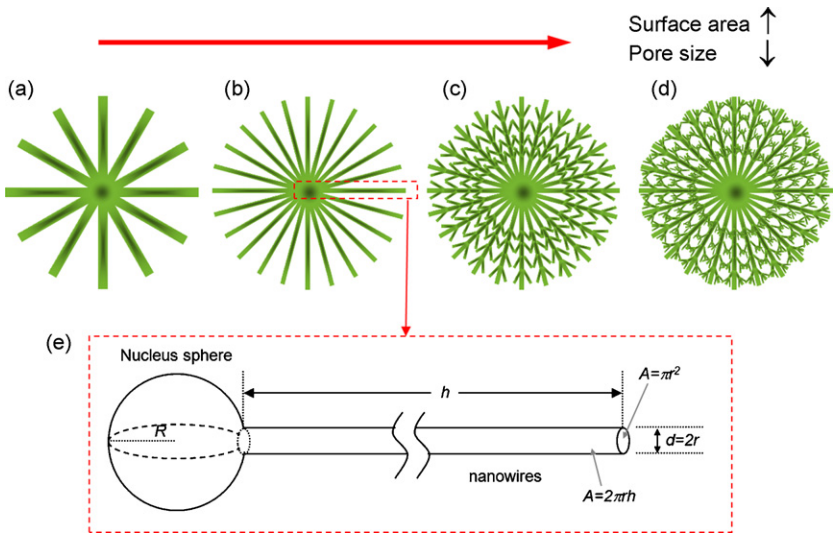

Fig. 11. (a–d) Hierarchical structures with various sizes and assembling configurations of nano-building blocks and (e) a simplified model to calculate the surface area of an urchin-like hierarchical microsphere.

the gas sensitivity. Moreover, complete depletion can be achieved by decreasing the thickness of the nano-building blocks to a level comparable with that of the electron depletion layer thickness. In the 2-3 flower-like structure, the high surface area and full electron depletion are determined by the smallest dimension of nanosheets, i.e., the thickness.

6.1.2. Porosity within hierarchical structures

In the hard aggregates of nanoparticles, the pore sizes decrease down to several nanometer or even sub-nanometer scale, which hampers the diffusion of analyte gas toward the inner part of the secondary particles [175]. In this condition, the inter-agglomerate contacts become more important than the inter-primary particle contacts and the apparent gas sensing characteristics show large variation [176]. Korotchenkov explained the negative effect of agglomeration in detail in his two review articles [28,177].

If nano-building blocks are assembled in a complex and dense manner in the hierarchical structures (for example, see Fig. 11(b)–(d)), the surface area will increase while the pore size and total volume decrease. However, in contrast to the agglomerated nanoparticles, hierarchical structures are generally assembled in highly periodic and porous manners. And the uniform thin/thick film sensors can be realized by sol deposition or screen printing of slurry containing hierarchical microspheres. Thus, in most cases, the gas diffusion toward the entire sensing surface is not hampered significantly even with the increased surface area due to the establishment of more complex hierarchical structures.

The present author and co-workers prepared 2-3 flower-like SnO_2 hierarchical microspheres by the heat treatment of hydrothermally synthesized, Sn_3O_4 2-3 hierarchical microspheres at 600 °C (Fig. 12(a)) [137]. The morphology of the building blocks within the SnO_2 hierarchical spheres could be manipulated from 2D nanosheets into 0D nanoparticles by controlling the composition of stock solution for hydrothermal synthesis (Fig. 12(b)). The specific surface areas of the hierarchical and dense SnO_2 microspheres were 46.4 and 34.7 m^2/g, respectively. The 2-3 flower-like, hierarchical SnO_2 microspheres contained a larger volume of mesopores and sub-micropores ranging in size from 4.5 to 20 nm and 33 to 100 nm, respectively (Fig. 12(c)). This clearly demonstrates that the hierarchical nanostructures provide a high surface area for gas sensing without sacrificing the porosity for effective gas diffusion.

6.2. Gas sensing characteristics of hierarchical oxide structures

Qin et al. [134] prepared 1-3 urchin-like SnO_2 hierarchical structures by hydrothermal reaction. The R_a/R_g ratio to 20 ppm CH_3COCH_3 at 290 °C was 5.5 with a very short gas response time of 7 s. Zhang et al. [140] prepared 1-2 dendrite-like, hierarchical structures through vapor phase transport with a Cu catalyst and prepared a gas sensor using a single ZnO dendrite. The dendrites had a bracken-like shape. The R_a/R_g ratio to 10 ppm H_2S at room temperature was ~10 and the gas response time was very short (15–20 s), considering the room-temperature gas sensing condition. Ponzoni et al. [152] reported that the WO_3 nanowire networks prepared by thermal evaporation of W powders showed a ~6-fold increase of resistance upon exposure to 50 ppb NO_2 at 300 °C. Gou et al. [156] synthesized hexapod-like nanostructures by hydrothermal route and measured the responses to various reducing gases. The gas responses to 50–1000 ppm of ethanol were 5–10-fold higher than those of commercial powders. The gas responses of these hexapod structures were also substantially enhanced in the sensing of various flammable, toxic and corrosive gases such as acetone, 92# gasoline, heptane, formaldehyde, toluene, acetic acid, and ammonia. These results indicate that the less agglomerated configuration of hierarchical structures enhances the gas response and increases the response speed.

Chen et al. [162] prepared SnO_2/α-F_2O_3 hierarchical heteronanostructures by growing SnO_2 branch nanorods on the side surface of α-F_2O_3 nanorods via a two-step hydrothermal reaction. In nano-crystalline gas sensor materials, the development of a hetero-junction between two different gas sensing materials often leads to a synergetic effect that enhances the gas sensing performance [178,179]. To date, various hierarchical heterostructures such as SnO_2/α-Fe_2O_3 [161,162], ZnO/SnO_2 [132], ZnO/Ga_2O_3 [164] and Ga_2O_3/In_2O_3 [165] have been prepared by two-step vapor phase growth. Thus, the sensitivity and selectivity can also be manipulated in the hierarchical heteronanostructures by controlling the component phases.

Fig. 13 shows the gas sensing transients of the 2-3 flower-like SnO_2 hierarchical microspheres and dense SnO_2 spheres that were shown in Fig. 12. The R_a/R_g ratios of the 2-3 hierarchical microspheres to 10–30 ppm C_2H_5OH at 400 °C ranged from 7.7 to 18, whereas those of the dense microspheres ranged from 4.6 to 7.9. The time to reach 90% variation in resistance (τ_{resp90}) upon exposure to

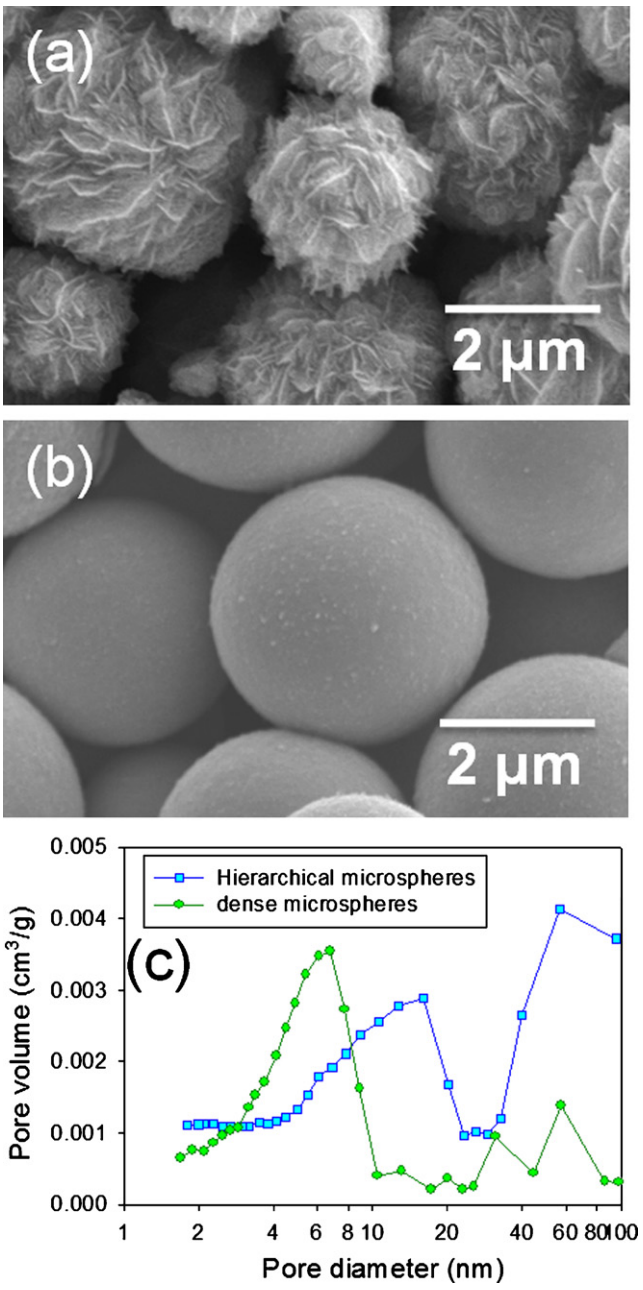

Fig. 12. SEM images of (a) flower-like SnO_2 hierarchical microspheres and (b) dense SnO_2 microspheres, and (c) the pore-size distributions of hierarchical and dense SnO_2 microspheres determined from nitrogen adsorption–desorption isotherm, according to [137].

30 ppm C_2H_5OH was dramatically decreased from 90 to 1 s by using the hierarchical structures. In addition, both the gas response and response kinetics upon exposure to H_2 and C_3H_8 were also greatly enhanced, which was attributed to the rapid gas diffusion onto the sensing surfaces via the well-aligned and nanoporous configuration of the hierarchical structures.

The present author and co-workers prepared 1-3 urchin-like In_2O_3 hierarchical microspheres by the solvothermal reaction of ethanol solution containing indium nitrate and L(+)-lysine and subsequent heat treatment at 600 °C (Fig. 14 presents an SEM image) [84]. In contrast, agglomerated In_2O_3 nanopowders were prepared from the solvothermal reaction of the solution containing indium nitrate and sodium dodecyl sulfate (Fig. 14 presents an SEM image). Fig. 14 shows the gas sensing transients that were normalized by the gas response. Here, the $(R_a/R_g)^{-1}$ ratio in the *y*-axis is the reciprocal of the gas response (R_a/R_g) so that the decrease and increase of $(R_a/R_g)^{-1}$ correspond to the decrease and increase, respectively, of the sensor resistances upon gas exposure. The $(R_a/R_g)^{-1}$ ratio of the hierarchical In_2O_3 sensor upon exposure to 30 ppm CO was ~0.32, which was significantly lower than ~0.75 of the agglomerated counterparts. This indicates that the gas response was enhanced ~2.3-fold by the use of the hierarchical structure. The τ_{resp90} value was dramatically shortened from 166 to 4 s by the use of the hierarchical structures as the sensor materials.

The gas sensing characteristics of hierarchical structures in the literature are summarized in Fig. 15. As stated before, for precise comparison, the literature data containing the gas response values (or response time) of both hierarchical structures and counterparts for comparison were estimated and plotted. The S_{HS}/S_{CP} ratios between the gas responses of the hierarchical structures and of the counterparts for comparison were all higher than unity (Fig. 15(a)), which confirmed the enhancement of gas response achieved by using the hierarchical structure. The ratio between the 90% response times of the counterparts for comparison and the hierarchical structure ($\tau_{resp90\text{-}CP}/\tau_{resp90\text{-}HS}$) ranged from 2 to ~90 (Fig. 15(b)), indicating a 2–90-fold increase in response speed. This is dramatic improvement in realizing the fast responding gas sensor. Both the S_{HS}/S_{CP} and $\tau_{resp90\text{-}CP}/\tau_{resp90\text{-}HS}$ ratios were >1 in the 2-3 flower-like SnO_2 hierarchical microspheres and 1-3 urchin-like In_2O_3 microspheres. These results clearly demonstrated that the hierarchical structures enhanced both the gas response and the gas response speed simultaneously and substantially.

7. Gas sensing mechanism of hierarchical and hollow nanostructures

The efforts to enhance the gas response by decreasing the particle sizes down to a scale of several nanometer are counteracted by the formation of aggregates due to Van der Waals attraction. The aggregation between primary particles is usually strong and irreversible, especially when the particle size becomes nanometer scale. The diffusion of analyte gas into the inner part of secondary aggregates is ineffective because of the small pore, long diffusion length, and tortuous pathway due to the heterogeneous pore-size distribution. Thus, only the resistance of the primary particles near the surface of the secondary particles is affected by the exposure to reducing gases and the primary particles in the core become inactive (Fig. 16(a)). This is the main reason for the low gas response in the aggregated nanoparticles. Furthermore, the sluggish gas diffusion through the pores between the primary nanoparticles greatly decreases the response speed.

In contrast, the gas diffusion length of hollow spheres is less than several tens of nanometers and most hierarchical structures provide well-defined and well-aligned micro-, meso-, and nanoporosity for effective gas diffusion (Fig. 16(b)). Therefore, the entire hollow and hierarchical nanostructures are quickly converted into a highly conducting state when exposed to the reducing gas in n-type semiconductor gas sensors. The resistance changes of the whole hollow and hierarchical nanostructures confirm the high gas response and the well-defined pore architectures induce the ultrafast gas response kinetics. Therefore, both a high gas response and a fast response can be achieved using hierarchical nanostructures.

8. Impact on chemical sensor technology and future direction

8.1. Impact on chemical sensor technology

The key advantages of oxide semiconductor gas sensors with hierarchical and hollow nanostructures are ultra fast response and

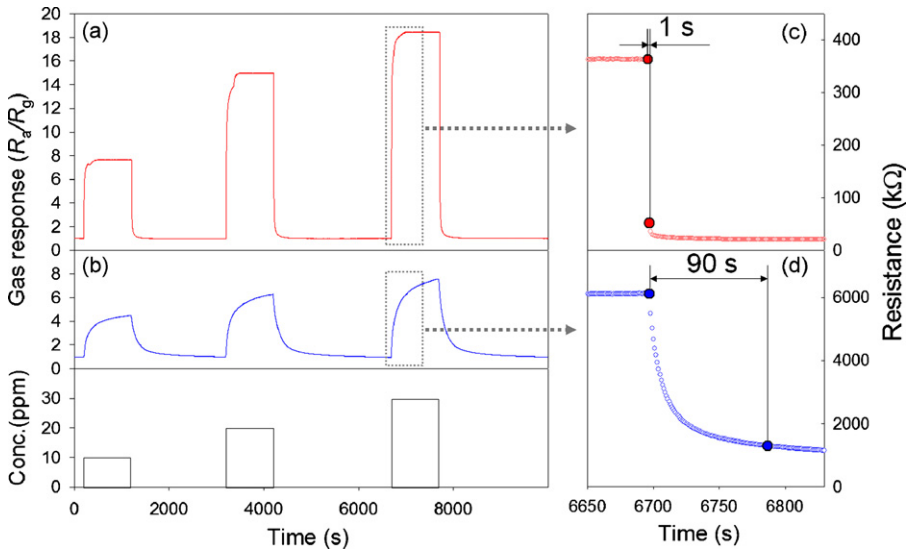

Fig. 13. Dynamic C_2H_5OH sensing characteristics at 400 °C: (a) gas response (R_a/R_g) of hierarchical SnO_2 spheres (Fig. 12(a)), (b) gas response (R_a/R_g) of dense SnO_2 microspheres (Fig. 12(b)), (c) change in the resistance of hierarchical spheres after exposure to 30 ppm C_2H_5OH, and (d) change in the resistance of dense spheres after exposure to 30 ppm C_2H_5OH (reproduced with permission from [137]).

high sensitivity. These are essential in the sensing of toxic, explosive, and dangerous gases. Especially, trace concentrations of toxic and explosive gases should be detected immediately or within a few seconds after the gas exposure in order to prevent catastrophic disasters. Gas sensors using hierarchical/hollow structures promise to satisfy these requirements.

The impact of fast responding gas sensors using hierarchical/hollow structures can also be found in the improved performance of artificial olfaction, i.e., electronic nose (eNOSE). Artificial olfaction usually discriminates and/or quantifies the complex chemical quantities that constitute the smell or odor by pattern recognition of the multivariate signals attained from sensor arrays. Although an algorithm for pattern recognition using the transient parts of sensor signals has been suggested [180,181], the precise time from exposure to gas is very difficult to define. Moreover, the transient of some sensors can fluctuate due to the instability of the sensor signals. Thus, the pattern recognition based on steady state signals will increase the reproducibility of the analysis results. When the sensors respond slowly to the gases, it took a long time to attain steady state signals from all the sensors. Even if most sensors respond quickly, the total sensing time of eNOSE remains limited by the slowest sensor component (Fig. 17). Therefore, a fast-responding and reliable eNOSE can be realized by developing various compositions of fast responding gas sensors using hierarchical and hollow spheres. This will open the possibility of real-time monitoring of the complex chemicals contained in smells and odors.

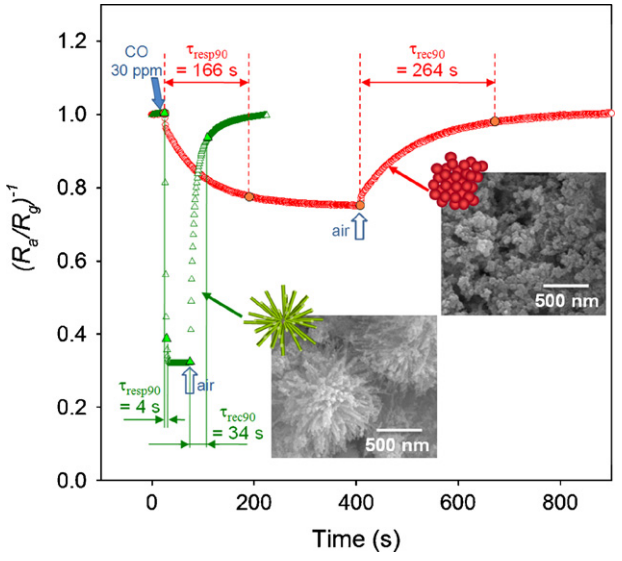

Fig. 14. Normalized gas sensing transients of In_2O_3 urchin-like particles and nanoparticles to 30 ppm CO at 400 °C, according to Ref. [84].

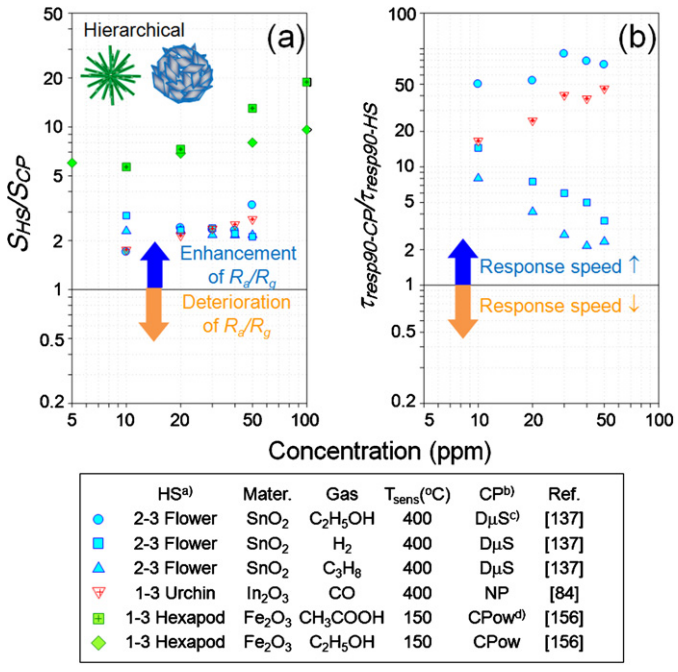

HS[a)]	Mater.	Gas	T_{sens}(°C)	CP[b)]	Ref.
2-3 Flower	SnO_2	C_2H_5OH	400	DμS[c)]	[137]
2-3 Flower	SnO_2	H_2	400	DμS	[137]
2-3 Flower	SnO_2	C_3H_8	400	DμS	[137]
1-3 Urchin	In_2O_3	CO	400	NP	[84]
1-3 Hexapod	Fe_2O_3	CH_3COOH	150	CPow[d)]	[156]
1-3 Hexapod	Fe_2O_3	C_2H_5OH	150	CPow	[156]

Fig. 15. (a) Ratios between the gas responses of hierarchical oxide structures ($S_{HS} = R_a/R_g$ (hierarchical structures)) and those of counterparts for comparison ($S_{CP} = R_a/R_g$ (counterparts)), and (b) ratios between the gas response times of counterparts for comparison ($\tau_{resp90\text{-}CP} = \tau_{resp90}$ (counterparts)) and those for hierarchical structures ($\tau_{resp90\text{-}HS} = \tau_{resp90}$ (hierarchical structures)). (a) HS: hierarchical structures, (b) CP: counterparts for comparison, (c) DμS: dense microspheres and (d) CPow: commercial powders. The data were estimated from Refs. [84,137,156].

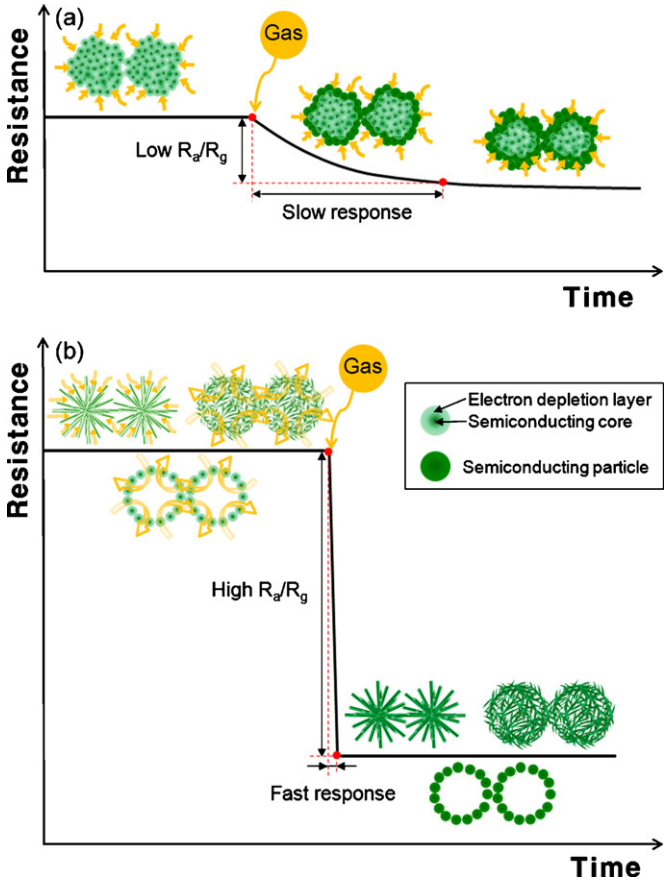

Fig. 16. Gas sensing principles of (a) agglomerated configuration of nanoparticles, and (b) hierarchical and hollow nanostructures.

8.2. Future directions

Various hierarchical and hollow structures of oxide gas sensor materials have been prepared. In order to optimize the gas response and response kinetics further, the more research is required. Remaining challenges include the preparation of multi-compositional, hierarchical/hollow structures and the functionalization of the surface using noble metal or metal oxide catalysts. These challenges are closely related to achieving selective gas detection and enhancing gas recovery kinetics.

The compositional variation of oxide semiconductor gas sensors is a representative approach to detect a specific gas [182,183]. The preparation of multi-compositional, hierarchical/hollow structures by one-pot, hydrothermal/solvothermal self-assembly is a challenging issue because the self-assembly reactions for the two different precursors differ from each other. However, careful selection of source materials based on detailed comprehension of the reaction chemistry enables the preparation of multi-compositional, hierarchical and hollow structures. The use of the two-step reaction promises to increase the convenience. The single oxide, hierarchical and hollow structures can be hydrothermally converted into the complex oxide forms by reacting with different cations under hydrothermal conditions [184]. Precise tuning of the composition in a hierarchical and hollow structure, therefore, can satisfy the three most important sensor characteristics: high sensitivity, fast response, and high selectivity.

The surface modification of hierarchical/hollow structures with noble or metal oxide catalysts is also very important to improve the gas sensing characteristics. In Fig. 14, the 90% recovery time (τ_{rec90}) of the hierarchical In_2O_3 microspheres (34 s) is markedly shorter than that of the agglomerated In_2O_3 nanoparticles (294 s), but still much longer than the very short response time (τ_{resp90} = 2 s). The marked shortening of the recovery time from 294 to 34 s was partially attributed to the enhanced gas diffusion through the well-defined and porous hierarchical structures. The recovery reaction involves the following serial reactions: the inward diffusion of oxygen toward the sensing surface, the adsorption of the oxygen molecule, the dissociation into atomic oxygen, and the ionization into the negatively charged oxygen. The oxygen diffusion can be regarded as fast, suggesting that the slow recovery results from the sluggish surface reactions. The addition of noble metal and/or metal oxide catalysts [46,47] to the oxide semiconductor gas sensor can quicken the recovery reaction. Moreover, the optimized design of catalysts materials greatly enhances not only the gas response [8,185–189] but also the selectivity [190,191]. It will therefore be worthwhile to investigate the functionalization of hierarchical/hollow structures with noble metals and/or metal oxides.

The fabrication of sensors using hierarchical nanostructures is also important. Various methods can be used to form the well-defined thin/thick films for gas sensors, which include the vapor phase deposition, solution deposition of sol solution, and screen printing of slurry. For the fabrication of eNOSE, the ink-jet printing [192] of different gas sensing materials on the electrode arrays can be employed. During the processing, the nano-porosity and packing density of hierarchical structures as well as the thickness of gas sensor film should be controlled precisely to attain reproducible and reliable gas sensing characteristics.

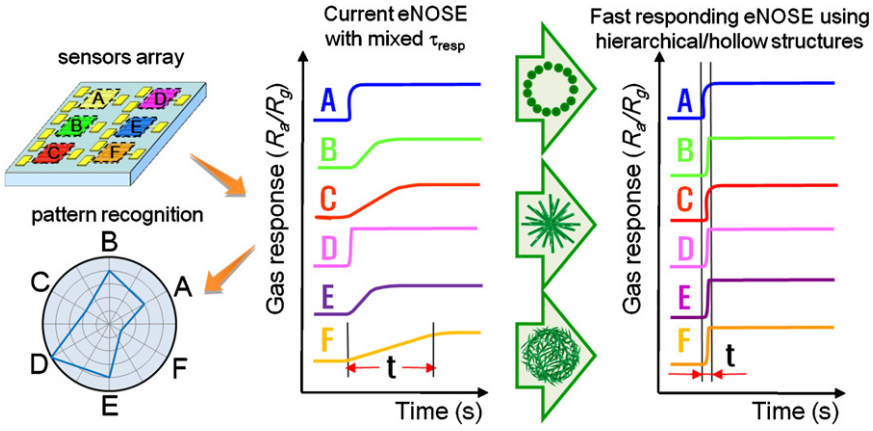

Fig. 17. The concept of fast responding artificial olfaction.

9. Conclusions

In oxide semiconductor gas sensors, achieving both high gas response and fast responding kinetics remains a challenging issue because any increase in the surface reaction sites attained by decreasing the particle sizes is usually hampered by the inevitable and irreversible, inter-primary particle aggregation. Hierarchical and hollow oxide nanostructures provide an effective gas diffusion path via well-aligned nanoporous architectures without sacrificing a high surface area, and therefore represent a very promising design option for gas sensors.

Hollow oxide structures can be prepared either by LbL coating, heterocoagulation and controlled hydrolysis using sacrificial templates, or by hydrothermal/solvothermal self-assembly reaction, spray pyrolysis, Ostwald ripening, and solid evacuation via the Kirkendall effect in the absence of templates. The principal parameters to determine the gas response and response speed in hollow structures are the thickness, permeability, and surface morphology of the shell layers, which are best optimized by manipulating the processing conditions or by using the expansion or decomposition of the templates during heat treatment. The gas responses of most hollow oxide structures were significantly higher than those of the counterparts for comparison (nanoparticles). This was attributed to the conversion of the entire hollow structures into conducting phase in n-type semiconductors and the rapid and effective gas diffusion through the thin and permeable shells.

Various hierarchical structures assembled from 0D, 1D, 2D, and 3D nano-building blocks can be prepared by vapor phase growth and hydrothermal/solvothermal self-assembly reaction. The main factors to determine the surface area of hierarchical structures are the smallest dimension and the assembly configuration of the nano-building blocks. The pore size and total pore volume of hierarchical structures can be decreased by increasing the packing density and complexity of the assembled nano-building blocks. Nevertheless, the well-aligned assembly of nanocrystalline building blocks in hierarchical structures does not usually restrict the diffusion of gases toward the entire sensing surface, whereas gas diffusion through the aggregated nanoparticles is difficult. The literature data confirm the successful attainment of both high gas response and rapid response speed by using various hierarchical structures.

Highly sensitive and fast responding gas sensors using hierarchical/hollow nanostructures can facilitate the instantaneous detection of toxic and dangerous gases, real-time gas monitoring, and fast responding artificial olfaction using steady-state signals.

Acknowledgements

This work was supported by the Korea Science and Engineering Foundation (KOSEF) National Research Laboratory (NRL) program grant funded by the Korean government (MEST) (No. R0A-2008-000-20032-0).

References

[1] N. Yamazoe, Toward innovations of gas sensor technology, Sens. Actuators B 108 (2005) 2–14.
[2] Y. Shimizu, M. Egashira, Basic aspects and challenges of semiconductor gas sensors, MRS Bull. 24 (1999) 18–24.
[3] C.O. Park, S.A. Akbar, Ceramics for chemical sensing, J. Mater. Sci. 38 (2003) 4611–4637.
[4] N. Barsan, U. Weimer, Conduction model of metal oxide gas sensors, J. Electroceram. 7 (2001) 143–167.
[5] X.-J. Huang, Y.-K. Choi, Chemical sensors based on nanostructured materials, Sens. Actuators B 122 (2007) 659–671.
[6] K. Soulantica, L. Erades, M. Sauvan, F. Senocq, A. Maisonnat, B. Chaudret, Synthesis of indium and indium oxide nanoparticles from indium cyclopentadienyl precursor and their application for gas sensing, Adv. Funct. Mater. 13 (2003) 553–557.
[7] A. Kolmakov, Y. Zhang, G. Cheng, M. Moskovits, Detection of CO and O_2 using tin oxide nanowire sensor, Adv. Mater. 15 (2003) 997–1000.
[8] A. Kolmakov, D.O. Klenov, Y. Lilach, S. Stemmer, M. Moskovits, Enhanced gas sensing by individual SnO_2 nanowires and nanobelts functionalized with Pd catalyst particles, Nano Lett. 5 (2005) 667–673.
[9] Y.-J. Choi, I.-S. Hwang, J.-G. Park, K.-J. Choi, J.-H. Park, J.-H. Lee, Novel fabrication of an SnO_2 nanowire gas sensor with high sensitivity, Nanotechnology 19 (2008) 095508.
[10] E. Comini, G. Faglia, M. Ferroni, G. Sberveglieri, Controlled growth and sensing properties of In_2O_3 nanowires, Cryst. Growth Des. 7 (2007) 2500–2504.
[11] I.D. Kim, A. Rothschild, B.H. Lee, D.Y. Kim, S.M. Jo, H.L. Tuller, Ultrasensitive chemiresistors based on electrospun TiO_2 nanofibers, Nano Lett. 6 (2006) 2009–2013.
[12] S. Yoo, S.A. Akbar, K.H. Sandhage, Nanocarving of bulk titania crystals into oriented arrays of single-crystal nanofibers via reaction with hydrogen-bearing gas, Adv. Mater. 16 (2004) 260–264.
[13] Y.L. Wang, X.C. Jiang, Y.N. Xia, A. Solution-Phase, Precursor route to polycrystalline SnO_2 nanowires that can be used for gas sensing under ambient conditions, J. Am. Chem. Soc. 125 (2003) 16176–16177.
[14] D. Zhang, Z. Liu, C. Li, T. Tang, X. Liu, S. Han, B. Lei, C. Zhou, Detection of NO_2 down to ppb levels using individual and multiple In_2O_3 nanowire devices, Nano Lett. 4 (2004) 1919–1924.
[15] I.-S. Hwang, Y.-S. Kim, S.-J. Kim, B.-K. Ju, J.-H. Lee, A facile fabrication of semiconductor nanowires gas sensor using PDMS patterning and solution deposition, Sens. Actuators B 136 (2009) 224–229.
[16] J.-H. Park, J.-H. Lee, Gas sensing characteristics of polycrystalline SnO_2 nanowires prepared by polyol method, Sens. Actuators B 136 (2009) 151–157.
[17] Y.-S. Kim, I.-S. Hwang, S.-J. Kim, C.-Y. Lee, J.-H. Lee, CuO nanowire gas sensors for air quality control in automotive cabin, Sens. Actuators B 135 (2008) 298–303.
[18] O.K. Varghese, D. Gong, M. Paulose, K.G. Ong, E.C. Dickey, C.A. Grimes, Extreme changes in the electrical resistance of titania nanotubes with hydrogen exposure, Adv. Mater. 15 (2003) 624–627.
[19] W.-Y. Li, L.-N. Xu, J. Chen, Co_3O_4, nanomaterials in lithium-ion batteries and gas sensors, Adv. Funct. Mater. 15 (2005) 851–857.
[20] Q. Dong, H. Su, J. Xu, D. Zhang, Influence of hierarchical nanostructures to the gas sensing properties of SnO_2 biomorphic films, Sens. Actuators B 123 (2007) 420–428.
[21] E. Comini, G. Faglia, G. Sberveglieri, Z. Pan, Z.L. Wang, Stable and highly sensitive gas sensors based on semiconducting oxide nanobelts, Appl. Phys. Lett. 81 (2002) 1869–1871.
[22] M. Law, H. Kind, B. Messer, F. Kim, P. Yang, Photochemical sensing of NO_2 with SnO_2 nanoribbon nanosensors at room temperature, Angew. Chem. Int. Ed. 41 (2002) 2405–2408.
[23] C.-S. Moon, H.-R. Kim, G. Auchterlonie, J. Drennan, J.-H. Lee, Highly sensitive and fast responding CO sensor using SnO_2 nanosheets, Sens. Actuators B 131 (2008) 556–564.
[24] C. Xiangfeng, J. Dongli, Z. Chenmou, The preparation and gas-sensing properties of $NiFe_2O_4$ nanocubes and nanorods, Sens. Actuators B 123 (2007) 793–797.
[25] C.N. Xu, J. Tamaki, N. Miura, N. Yamazoe, Grain size effects on gas sensitivity of porous SnO_2-based elements, Sens. Actuators B 3 (1991) 147–155.
[26] B.-K. Kim, S.-D. Choi, SnO_2 thin film gas sensor fabricated by ion beam deposition, Sens. Actuators B 98 (2004) 239–246.
[27] M. Shoyama, N. Hashimoto, Effect of poly ethylene glycol addition on the microstructure and sensor characteristics of SnO_2 thin films prepared by sol–gel method, Sens. Actuators B 93 (2003) 585–589.
[28] G. Korotchenkov, Gas response control through structural and chemical modification of metal oxide films: state of the art and approaches, Sens. Actuators B 107 (2005) 209–232.
[29] E. Comini, C. Bratto, G. Faglia, M. Ferroni, A. Vomiero, G. Sberveglieri, Quasi-one dimensional metal oxide semiconductors: preparation and characterization and application as chemical sensors, Prog. Mater. Sci. 54 (2009) 1–67.
[30] A. Kolmakov, M. Moskovits, Chemical sensing and catalyst by one-dimensional metal oxide nanostructures, Annu. Rev. Mater. Res. 34 (2004) 151–180.
[31] Y. Xia, P. Yang, Y. Sun, Y. Wu, B. Mayers, B. Gates, Y. Yin, F. Kim, H. Yan, One-dimensional nanostructures: synthesis, characterization, and applications, Adv. Mater. 15 (2003) 353–389.
[32] U. Ciesla, F. Schüth, Ordered mesoporous materials, Micropor. Mesopor. Mater. 27 (1999) 131–149.
[33] P. Yang,.D. Zhao, D.I. Margolese, B.F. Chmelka, G.D. Stucky, Generalized syntheses of large-pore mesoporous metal oxides with semicrystalline frameworks, Nature 396 (1998) 152–155.
[34] J.K. Shon, S.S. Kong, Y.S. Kim, J.-H. Lee, W.K. Park, S.C. Park, J.M. Kim, Solvent-free infilteration method for mesoporous SnO_2 using mesoporous silica templates, Micropor. Mesopor. Mater. 120 (2009) 441–446.
[35] Y. Shimizu, T. Hyodo, M. Egashira, Mesoporous semiconducting oxides for gas sensor application, J. Eur. Ceram. Soc. 24 (2004) 1389–1398.
[36] Y. Shimizu, A. Jono, T. Hyodo, M. Egashira, Preparation of large mesoporous SnO_2 powders for gas sensor application, Sens. Actuators B 108 (2005) 56–61.
[37] W. Yue, W. Zhou, Crystalline mesoporous metal oxide, Progr. Nat. Sci. 18 (2008) 1329–1338.
[38] G.S. Devi, T. Hyodo, Y. Shimizu, M. Egashira, Synthesis of mesoporous TiO_2-based powders and their gas-sensing properties, Sens. Actuators B 87 (2002) 122–129.

[39] T. Hyodo, Y. Shimizu, M. Egashira, Gas-sensing properties of ordered mesoporous SnO_2 and effects of coating thereof, Sens. Actuators B 93 (2003) 590–600.
[40] T. Wagner, T. Waitz, J. Roggenbuck, M. Fröba, C.-D. Kohl, M. Tiemann, Ordered mesoporous ZnO for gas sensing, Thin Solid Film 515 (2007) 8360–8363.
[41] J. Yang, K. Hidajat, S. Kawi, Synthesis of nano-SnO_2/SBA-15 composite as a highly sensitive semiconductor oxide gas sensor, Mater. Lett. 62 (2008) 1441–1443.
[42] T. Wagner, C.-D. Kohl, M. Fröba, M. Tiemann, Gas sensing properties of ordered mesoporous SnO_2, Sensors 6 (2006) 318–323.
[43] C.-Y. Liu, C.-F. Chen, J.-P. Leu, Fabrication and CO sensing properties of mesostructured ZnO gas sensors, Electrochem. Solid. State Lett. 156 (2009) J16–J19.
[44] T. Waitz, T. Wagner, T. Sauerwald, C.-D. Kohl, M. Tiemann, Ordered mesoporous In_2O_3: synthesis by structure replication and application as a methane gas sensor, Adv. Funct. Mater. 19 (2009) 653–661.
[45] Q. Liu, W.-M. Zhang, Z.-M. Cui, B. Zhang, L.-J. Wan, W.-G. Song, Aqueous route for mesoporous metal oxides using inorganic metal source and their applications, Micropor. Mesopor. Mater. 100 (2007) 233–240.
[46] E. Rossinyol, A. Prim, E. Pellicer, J. Rodríguez, F. Peiró, A. Cornet, J.R. Morante, B. Tian, T. Bo, D. Zhao, Mesostructured pure and copper-catalyzed tungsten oxide for NO_2 detection, Sens. Actuators B 126 (2007) 18–23.
[47] E. Rossinyol, A. Prim, E. Pellicer, J. Arbiol, F. Hernández-Ramírez, F. Peiró, A. Cornet, J.R. Morante, L.A. Solovyov, B. Tian, T. Bo, D. Zhao, Synthesis and characterization of chromium-doped mesoporous tungsten oxide for gas sensing applications, Adv. Funct. Mater. 17 (2007) 1801–1806.
[48] F. Caruso, Nanoengineering of particle surfaces, Adv. Mater. 13 (2001) 11–22.
[49] F. Caruso, R.A. Caruso, H. Möhwald, Nanoengineering of inorganic and hybrid hollow spheres by colloidal templating, Science 282 (1998) 1111–1114.
[50] R. Meyer Jr., H. Weitzing, Q. Xu, Q. Zhang, R.E. Newnham, Lead zirconate titanate hollow-sphere transducers, J. Am. Ceram. Soc. 77 (1994) 1669.
[51] S. Han, B. Jang, T. Kim, S.M. Oh, T. Hyeon, Simple synthesis of hollow tin dioxide microspheres and their applications to lithium-ion battery anodes, Adv. Funct. Mater. 15 (2005) 1845–1850.
[52] X.W. Lou, L.A. Archer, Z. Yang, Hollow micro-/nanostructures: synthesis and applications, Adv. Mater. 20 (2008) 3987–4019.
[53] T. Hyodo, K. Sasahara, Y. Shimizu, M. Egashira, Preparation of macroporous SnO_2 films using PMMA microspheres and their sensing properties to NO_x and H_2, Sens. Actuators B 106 (2005) 580–590.
[54] Y. Tan, C. Li, Y. Wang, J. Tang, X. Ouyang, Fast-response and high sensitivity gas sensors based on SnO_2 hollow spheres, Thin Solid Films 516 (2008) 7840–7843.
[55] J. Zhang, S. Wang, Y. Wang, Y. Wang, B. Zhu, H. Xia, X. Guo, S. Zhang, W. Huang, S. Wu, NO_2 sensing performance of SnO_2 hollow-sphere sensor, Sens. Actuators B 135 (2009) 610–617.
[56] Z. Zhong, Y. Yin, B. Gates, Y. Xia, Preparation of mesoscale hollow spheres of TiO_2 and SnO_2 by templating against crystalline arrays of polystyrene beads, Adv. Mater. 12 (2000) 206–209.
[57] C.J. Martinez, B. Hockey, C.B. Montgomery, S. Semancik, Porous tin oxide nanostructured microspheres for sensor applications, Langmuir 21 (2005) 7937–7944.
[58] H.X. Yang, J.F. Qian, Z.X. Chen, X.P. Ai, Y.L. Cao, Multilayered nanocrystalline SnO_2 hollow microspheres synthesized by chemically induced self-assembly in the hydrothermal environment, J. Phys. Chem. C 111 (2007) 14067–14071.
[59] Q. Zhao, Y. Gao, X. Bai, C. Wu, Y. Xie, Facile synthesis of SnO_2 hollow nanospheres and applications in gas sensors and electrocatalysts, Eur. J. Inorg. Chem. (2008) 1643–1648.
[60] H. Wang, J. Liang, H. Fan, B. Xi, M. Zhang, S. Xiong, Y. Zhu, Y. Qian, Synthesis and gas sensitivities of SnO_2 nanorods and hollow microspheres, J. Solid State Chem. 181 (2008) 122–129.
[61] X.W. Lou, Y. Wang, C. Yuan, J.Y. Lee, L.A. Archer, Template-free synthesis of SnO_2 hollow nanostructures with high lithium capacity, Adv. Mater. 18 (2006) 2325–2329.
[62] D. Wang, J. Xu, Q. Pan, Fabrication and gas-sensing properties of hollow SnO_2 microspheres, Chem. Lett. 37 (2008) 1086–1087.
[63] M.V. Cabanas, G. Delabouglise, M. Labeau, M. Vallet-Regí, Application of a modified ultrasonic aerosol device to the synthesis of SnO_2 and Pt/SnO_2 for gas sensors, J. Solid State Chem. 144 (1999) 86–90.
[64] H.-P. Cong, S.-H. Yu, Hybrid-dye hollow spheres with new optical properties from a self-assembly process based on Evans blue dye and cetyltrimethylammonium bromide, Adv. Funct. Mater. 17 (2007) 1814–1820.
[65] Q. Wu, X. Chen, P. Zhang, Y. Han, X. Chen, Y. Yan, S. Li, Amino acid-assisted synthesis of ZnO hierarchical architectures and their novel photocatalytic activities, Cryst. Growth Des. 8 (2008) 3010–3018.
[66] J. Tao, X. Chen, Y. Sun, Y. Shen, N. Dai, Controllable preparation of ZnO hollow microspheres by self-assembled block copolymer, Colloids Surf. A 330 (2008) 67–71.
[67] Y. Zhang, E.-W. Shi, Z.-Z. Chen, B. Xiao, Fabrication of ZnO hollow nanospheres and "jingle bell" shaped nanospheres, Mater. Lett. 62 (2008) 1435–1437.
[68] X.L. Zhang, R. Qiao, J.C. Kim, Y.S. Kang, Inorganic cluster synthesis and characterization of transition-metal-doped ZnO hollow spheres, Cryst. Growth Des. 8 (2008) 2609–2613.
[69] M. Mo, J.C. Yu, L. Zhang, S.A. Li, Self-assembly of ZnO nanorods and nanosheets into hollow microhemispheres and microspheres, Adv. Mater. 17 (2005) 756–760.
[70] H. Zhang, J. Wu, C. Zhai, N. Du, X. Ma, D. Yang, From ZnO nanorods to 3D hollow mircohemispheres: solvothermal synthesis, photoluminescence and gas sensor properties, Nanotechnology 18 (2007) 455604.
[71] Y. Tian, H. Lu, D. Wang, J. Li, M. Shuai, Q. Fu, Synthesis of zinc oxide hollow spherical structure via precursor-template and formation mechanism, J. Phys. Soc. Jpn. 77 (2008) 07463.
[72] Z. Xingfu, H. Zhaolin, F. Yiqun, D. Weiping, X. Nanping, Hollow microsphere assembly of ZnO nanosheets, Mater. Chem. Phys. 112 (2008) 592–595.
[73] X.-L. Li, T.-J. Lou, X.-M. Sun, Y.-D. Li, Highly sensitive WO_3 hollow-sphere gas sensors, Inorg. Chem. 43 (2004) 5442–5449.
[74] J. Yu, H. Yu, H. Guo, M. Li, S. Mann, Spontaneous formation of tungsten trioxide sphere-in-shell superstructure by chemically induced self-transformation, Small 4 (2008) 87–91.
[75] Z. Zhao, T.L.Y. Cheung, Z. Zhang, D.H.L. Ng, J. Yu, Facile preparation of strontium tungstate and tungsten trioxide hollow spheres, J. Am. Ceram. Soc. 89 (2006) 2960–2963.
[76] D. Chen, J. Ye, Hierarchical WO_3 hollow shells: dendrite, sphere, dumbbell, and their photocatalytic properties, Adv. Funct. Mater. 18 (2008) 1922–1928.
[77] F. Caruso, X. Shi, R.A. Caruso, A. Susha, Hollow titania spheres from layered precursor deposition on sacrificial colloidal core particles, Adv. Mater. 13 (2001) 740–744.
[78] G. Li, C. Liu, Y. Liu, Facile fabrication of hollow mono-dispersed TiO_2 spheres in an aqueous solution, J. Am. Ceram. Soc. 90 (2007) 2667–2669.
[79] J.-Y. Lee, J.-H. Lee, S.-H. Hong, Y.K. Lee, J.-Y. Choi, Coating of TiO_2 nano-layer on spherical Ni particles using novel sol–gel route, J. Mater. Res. 19 (2004) 1669–1675.
[80] J.-Y. Lee, J.-H. Lee, S.-H. Hong, Y.K. Lee, J.-Y. Choi, Coating of $BaTiO_3$ nano-layer on spherical Ni powders for MLCC, Adv. Mater. 15 (2003) 1655–1658.
[81] V. Jokanović, A.M. Spasić, D. Uskoković, Designing of nanostructured hollow TiO_2 spheres obtained by ultrasonic spray pyrolysis, J. Colloid Interface Sci. 278 (2004) 342–352.
[82] H. Yang, H.C. Zeng, Preparation of hollow anatase TiO_2 nanospheres via Ostwald ripening, J. Phys. Chem. B. 108 (2004) 3492–3495.
[83] I.-D. Kim, A. Rothschild, D.-J. Yang, H.L. Tuller, Macroporous TiO_2 thin film gas sensors obtained using colloidal templates, Sens. Actuators B 130 (2008) 9–13.
[84] K.-I. Choi, H.-R. Kim, J.-H. Lee, Enhanced CO sensing characteristics of hierarchical and hollow In_2O_3 microspheres, Sens. Actuators B. 138 (2009) 497–503.
[85] B. Li, Y. Xie, M. Jing, G. Rong, Y. Tang, G. Zhang, In_2O_3 hollow microspheres: synthesis from designed $In(OH)_3$ precursors and applications in gas sensors and photocatalysts, Langmuir 22 (2006) 9380–9385.
[86] H. Shiho, N. Kawahashi, Iron compounds as coatings on polystyrene latex, J. Colloid Interface Sci. 226 (2000) 91–97.
[87] F. Caruso, M. Spasova, A. Susha, M. Giersig, R.A. Caruso, Magnetic nanocomposite particles and hollow spheres constructed by a sequential layering approach, Chem. Mater. 13 (2001) 109–116.
[88] B. Jia, L. Gao, Morphological transformation of Fe_3O_4 spherical aggregates from solid to hollow and their self-assembly under an external magnetic field, J. Phys. Chem. C 112 (2008) 666–671.
[89] W.S. Choi, Y. Koo, Z. Zhongbin, Y. Li, D.-Y. Kim, Template synthesis of porous capsules with a controllable surface morphology and their application as gas sensors, Adv. Funct. Mater. 17 (2007) 1743–1749.
[90] H. Zhang, Q. Zhu, Y. Zhang, Y. Wang, L. Zhao, B. Yu, One-pot synthesis and hierarchical assembly of hollow Cu_2O microspheres with nanocrystals-composed porous multishell and their gas-sensing properties, Adv. Funct. Mater. 17 (2007) 2766–2771.
[91] Y. Zhang, X. He, J. Li, H. Zhang, X. Gao, Gas-sensing properties of hollow and hierarchical copper oxide microspheres, Sens. Actuators B 128 (2007) 293–298.
[92] S. Gao, S. Yang, J. Shu, S. Zhang, Z. Li, K. Jiang, Green fabrication of hierarchical CuO hollow micro/nanostructures and enhanced performance as electrode materials for lithium-ion batteries, J. Phys. Chem. C 112 (2008) 19324–19328.
[93] D. Wang, C. Song, Z. Hu, S. Fu, Fabrication of hollow spheres and thin films of nickel hydroxide and nickel oxide with hierarchical structures, J. Phys. Chem. B 109 (2005) 1125–1129.
[94] X.L. Yu, Y. Wang, H.L.W. Chan, C.B. Cao, Novel gas sensoring materials based on CuS hollow spheres, Micropor. Mesopor. Mater. 118 (2009) 423–426.
[95] W.W. Wang, Y.J. Zhu, L.X. Yang, ZnO–SnO_2 hollow spheres and hierarchical nanosheets: hydrothermal preparation, formation mechanism, and photocatalytic properties, Adv. Funct. Mater. 17 (2007) 59–64.
[96] N. Kawahashi, E. Matijević, Preparation and properties of uniform coated colloidal particles, J. Colloid Interface Sci. 138 (1990) 534–542.
[97] S. Radice, P. Kern, H. Dietsch, S. Mishchler, J. Michler, Method for functionalization of microsized polystyrene beads with titania nanoparticles for cathodic electrophoretic deposition, J. Colloid Interface Sci. 318 (2008) 264–270.
[98] S. Somiya, R. Roy, Hydrothermal synthesis of fine oxide particles, Bull. Mater. Sci. 23 (2000) 453–460.
[99] W.-T. Yao, S.-H. Yu, Recent advances in hydrothermal syntheses of low dimensional nanoarchitectures, Int. J. Nanotechnol. 4 (2007) 129–162.
[100] K. Byrappa, T. Adschiri, Hydrothermal technology for nanotechnology, Progr. Cryst. Growth Charact. Mater. 53 (2007) 117–166.
[101] M. Rajamathi, R. Seshadri, Oxide and chalgogenide nanoparticles from hydrothermal/solvothermal reactions, Curr. Opin. Solid State Mater. Sci. 6 (2002) 337–345.
[102] G.L. Messing, S.-C. Zhang, G.V. Jayanthi, Ceramic powder synthesis by spray pyrolysis, J. Am. Ceram. Soc. 76 (1993) 2707–2726.

[103] S. Jain, D.J. Skamser, T.T. Kodas, Morphology of single-component particles produced by spray pyrolysis, Aerosol Sci. Technol. 27 (1997) 575–590.
[104] S.H. Ju, Y.C. Kang, Fine-sized $LiBi_{0.8}Co_{0.15}Mn_{0.05}O_2$ cathode powders prepared by combined process of gas-phase reaction and solid-state reaction methods, J. Power Sources 178 (2008) 387–392.
[105] S.C. Zhang, G.L. Messing, W. Huebner, $YBa_2Cu_3O_{7-x}$ superconductor powder synthesis by spray pyrolysis of organic acid solutions, J. Aerosol Sci. 22 (1991) 585–599.
[106] J.-H. Lee, S.-J. Park, Preparation of spherical TiO_2/SnO_2 powders by ultrasonic spray pyrolysis and its spinodal decomposition, J. Mater. Sci.: Mater. Electron. 4 (1993) 254–258.
[107] H.-B. Kim, J.-H. Lee, S.-J. Park, Preparation of spherical $Pb(Zr,Ti)O_3$ powders by ultrasonic spray pyrolysis, J. Mater. Sci.: Mater. Electron. 6 (1995) 84–89.
[108] S.Y. Cho, J.-H. Lee, S.-J. Park, Preparation of spherical $(Zr,Sn)TiO_4$ powders by ultrasonic spray pyrolysis, J. Mater. Sci. 30 (1995) 3274–3278.
[109] H.C. Zeng, Synthetic architecture of interior space for inorganic nanostructures, J. Mater. Chem. 16 (2006) 649–662.
[110] Y. Yin, R.M. Rioux, C.K. Erdonmez, S. Hughes, G.A. Somorjai, A.P. Alivisatos, Formation of hollow nanocrystals through the nanoscale Kirkendall effect, Science 30 (2004) 711–714.
[111] H.J. Fan, Y. Gösele, M. Zacharias, Formation of nanotubes and hollow nanoparticles based on Kirkendall and diffusion processes: a review, Small 3 (2007) 1660–1671.
[112] B. Liu, H.C. Zeng, Fabrication of ZnO "Dandelions" via a modified Kirkendall process, J. Am. Ceram. Soc. 126 (2004) 16744–16746.
[113] P.I. Gaiduk, J.L. Hansen, A.N. Larsen, Synthesis and analysis of hollow SnO_2 nanoislands, Appl. Phys. Lett. 92 (2008) 193112.
[114] V. Brinzari, G. Korotchenkov, V. Golovanov, Factors influencing the gas sensing characteristics of tin dioxide films deposited by spray pyrolysis: understanding and possibilities of control, Thin Solid Films 391 (2001) 167–175.
[115] G. Sakai, N. Matsunaga, K. Shimanoe, N. Yamazoe, Theory of gas-diffusion controlled sensitivity for thin film semiconductor gas sensor, Sens. Actuators B 80 (2001) 125–131.
[116] L. Bruno, C. Pijolat, R. Lalauze, Tin dioxide thin-film gas sensor prepared by chemical vapour deposition: influence of grain size and thickness on the electrical properties, Sens. Actuators B 18–19 (1994) 195–199.
[117] G. Korochenkov, V. Brinzari, A Cerneavschi, M. Ivanov, V. Golovanoc, A. Cornet, J. Morante, A. Cabot, J. Arbiol, The influence of film structure on In_2O_3 gas response, Thin Solid Film 460 (2004) 315–323.
[118] N. Kawasashi, E. Matijević, Preparation of hollow spherical particles of yttrium compounds, J. Colloid Interface Sci. 143 (1991) 103–110.
[119] H.-R. Kim, K.-I. Choi, J.-H. Lee, unpublished work.
[120] K. Hieda, T. Hyodo, Y. Shimizu, M. Egashira, Preparation of porous tin oxide by ultrasonic spray pyrolysis and their application to sensor materials, Sens. Actuators B 133 (2008) 144–150.
[121] I.-D. Kim, A. Rothschild, T. Hyodo, H.L. Tuller, Microsphere templating as means of enhancing surface activity and gas sensitivity of $CaCu_3Ti_4O_{12}$ thin films, Nano Lett. 6 (2006) 193–198.
[122] Y.-K. Jun, H.-S. Kim, J.-H. Lee, S.-H. Hong, CO sensing performance in micro-arc oxidized TiO_2 films for air quality control, Sens. Actuators B 120 (2006) 69–73.
[123] I.T. Weber, R. Andrade, E.R. Leite, E. Longo, A study of the $SnO_2{\cdot}Nb_2O_5$ system for an ethanol vapor sensor: a correlation between microstructure and sensor performance, Sens. Actuators B 72 (2001) 180–183.
[124] V.R. Shinde, C.D. Lokhande, R.S. Mane, S.-H. Han, Use of chemically synthesized ZnO thin films as a liquefied petroleum gas sensor, Mater. Sci. Eng. B 137 (2007) 119–125.
[125] T.P. Chou, Q. Zhang, E. Fryxell, G. Cao, Hierarchically structured ZnO film for dye-sensitized solar cells with enhanced energy conversion efficiency, Adv. Mater. 19 (2007) 2588–2592.
[126] J.-S. Hu, L.-S. Zhong, W.-G. Song, L.-J. Wan, Synthesis of hierarchically structured metal oxides and their application in heavy metal ion removal, Adv. Mater. 90 (2008) 2977–2982.
[127] A.-M. Cao, J.-S. Ju, H.-P. Liang, W.-G. Song, L.-J. Wan, X.-L. He, X.-G. Gao, S.-H. Xia, Hierarchically structured cobalt oxide (Co_3O_4): the morphology control and its potential in sensors, J. Phys. Chem. B. 110 (2006) 15858–15863.
[128] L. Zhang, W. Wang, Z. Chen, L. Zhou, H. Xu, W. Zhu, Fabrication of flower-like Bi_2WO_6 superstructures as high performance visible-light driven photocatalysts, J. Mater. Chem. 17 (2007) 2526–2532.
[129] H. Xu, Z. Zheng, L. Zhang, H. Zhang, F. Deng, Hierarchical chlorine-doped rutile TiO_2 spherical clusters of nanorods: large-scale synthesis and high photocatalytic activity, J. Solid State Chem. 181 (2008) 2516–2522.
[130] S. Sun, W. Wang, H. Xu, L. Zhou, M. Shang, L. Zhang, $Bi_5FeTi_3O_{15}$ hierarchical microflowers: hydrothermal synthesis, growth mechanism, and associated visible-light-driven photocatalysts, J. Phys. Chem. C 112 (2008) 17835–17843.
[131] E. Hosono, S. Fujihara, I. Honma, M. Ichihara, H.S. Zhou, Fabrication of nano/micro hierarchical Fe_2O_3/Ni micrometer-wire structure and characteristics for high rate Li rechargeable battery, J. Electrochem. Soc. 153 (2006) A1273–A1278.
[132] S. Sun, G. Meng, G. Zhang, J.P. Masse, L. Zhang, Controlled growth of SnO_2 hierarchical nanostructures by a multistep thermal vapor deposition process, J. Eur. Chem. 13 (2007) 9087–9092.
[133] Q. Wang, K. Yu, F. Xu, Synthesis and filed emission of two kinds of hierarchical SnO_2 nanostructures, Solid State Commun. 143 (2007) 260–263.
[134] L. Qin, J. Xu, X. Dong, Q. Pan, Z. Cheng, Q. Xiang, F. Li, The template-free synthesis of square-shaped SnO_2 nanowires: the temperature effect and acetone gas sensors, Nanotechnology 19 (2008) 185705.
[135] G. Cheng, K. Wu, P. Zhao, Y. Cheng, X. He, K. Huang, Controlled growth of oxygen-deficient tin oxide nanostructures via a solvothermal approach in mixed solvents and their optical properties, Nanotechnology 18 (2007) 355604.
[136] H. Ohgi, T. Maeda, E. Hosono, S. Fujihara, H. Imai, Evolution of nanoscale SnO_2 grains, flakes, and plates into versatile particles and films through crystal growth in aqueous solution, Cryst. Growth Des. 5 (2005) 1079–1083.
[137] H.-R. Kim, K.-I. Choi, J.-H. Lee, S.A. Akbar, Highly sensitive and ultra-fast responding gas sensors using self-assembled hierarchical SnO_2 spheres, Sens. Actuators B 136 (2009) 138–143.
[138] Y. Yan, L. Zhou, L. Yu, Y. Zhang, Morphology evolution of hierarchical ZnO nanostructures modulated by supersaturation and growth temperature, J. Appl. Phys. 93 (2008) 457–465.
[139] M.S. Mo, S.H. Lim, Y.W. Mai, R.K. Zheng, S.P. Ringer, In situ self-assembly of thin ZnO nanoplatelets into hierarchical mesocrystal microtubules with surface grafting of nanorods: a general strategy towards hollow mesocrystal structures, Adv. Mater. 20 (2008) 339–342.
[140] N. Zhang, K. Yu, Q. Li, Z.Q. Zhu, Q. Wan, Room-temperature high-sensitivity H_2S gas sensor based on dendritic ZnO nanostructures with macroscale in appearance, J. Appl. Phys. 103 (2008) 104305.
[141] P.-S. Cho, K.-W. Kim, J.-H. Lee, NO_2 sensing characteristics of ZnO nanorods prepared by hydrothermal method, J. Electroceram. 17 (2006) 975–978.
[142] W. Peng, S. Qu, G. Cong, Z. Wang, Synthesis and structures of morphology-controlled ZnO nano- and microcrystals, Cryst. Growth Des. 6 (2006) 1518–1522.
[143] H. Zhu, J.F. Huang, Z. Pan, S. Dai, Ionothermal synthesis of hierarchical ZnO nanostructures from ionic-liquid precursors, Chem. Mater. 18 (2006) 4473–4477.
[144] P. Zhu, J. Zhang, Z. Wu, Z. Zhang, Microwave-assisted synthesis of various ZnO hierarchical nanostructures: effects of heating parameters of microwave oven, Cryst. Growth Des. 8 (2008) 3148–3153.
[145] Y. Li, M. Zheng, L. Ma, M. Zhong, W. Shen, Fabrication of hierarchical ZnO architectures and their superhydrophobic surfaces with strong adhesive force, Inorg. Chem. 47 (2008) 3140–3143.
[146] X. Zeng, J. Yuan, Z. Wang, L. Zhang, Nanosheet-based microspheres of Eu^{3+}-doped ZnO with efficient energy transfer from ZnO to Eu^{3+} at room temperature, Adv. Mater. 19 (2007) 4510–4514.
[147] X. Zeng, J. Yuan, L. Zhang, Synthesis and photoluminescent properties of rare earth doped ZnO hierarchical microspheres, J. Phys. Chem. C 112 (2008) 3503–3508.
[148] D.F. Zhang, L.D. Sun, J. Zhang, Z.G. Yan, C.H. Yan, Hierarchical construction of ZnO Architectures promoted by heterogeneous Nucleation, Cryst. Growth Des. 8 (2008) 3609–3615.
[149] Y. Baek, Y. Song, K. Yong, A novel heteronanostructure system: hierarchical W nanothorn arrays on WO_3 nanowhiskers, Adv. Mater. 18 (2006) 3105–3110.
[150] Z. Gu, T. Zhai, B. Gao, X. Sheng, Y. Wang, H. Fu, Y. Ma, J. Yao, Controllable assembly of WO_3 nanorods/nanowires into hierarchical nanostructures, J. Phys. Chem. 110 (2006) 23829–23836.
[151] J. Zhou, Y. Ding, S.Z. Deng, L. Gong, N.S. Xu, Z.L. Wang, Three-Dimensional yungsten oxide nanowire networks, Adv. Mater. 17 (2005) 2107–2110.
[152] A. Ponzoni, E. Comini, G. Sberveglieri, J. Zhou, S.Z. Deng, N.S. Xu, Y. Ding, Z.L. Wang, Ultrasensitive and highly selective gas sensors using three-dimensional tungsten oxide nanowire networks, Appl. Phys. Lett. 88 (2006) 203101.
[153] Y. Takezawa, H. Imai, Bottom-up synthesis of titanate nanosheets with hierarchical structures and a high specific surface area, Small 3 (2006) 390–393.
[154] X. Hu, J.C. Yu, J. Gong, Fast production of self-assembled hierarchical α-Fe_2O_3 nanoarchitectures, J. Phys. Chem. C 111 (2007) 11180–11185.
[155] B. Xue, R. Liu, Z.-D. Xu, Y.-F. Zeng, Microwave fabrication and magnetic property of hierarchical spherical α-Fe_2O_3 nanostructures, Chem. Lett. 37 (2008) 1058–1059.
[156] X. Gou, G. Wang, X. Kong, D. Wexler, J. Horvat, J. Yang, J. Park, Flutelike porous hematite nanorods and branched nanostructures: synthesis, characterization and application for gas-sensing, Chem. Eur. J. 14 (2008) 5996–6002.
[157] D. Keyson, D.P. Volanti, L.S. Cavalcante, A.Z. Simões, J.A. Varela, E. Longo, CuO urchin-nanostructures synthesized from a domestic hydrothermal microwave method, Mater. Res. Bull. 43 (2008) 771–775.
[158] Z. Yang, J. Xu, W. Zhang, A. Liu, S. Tang, Controlled synthesis of CuO nanostructures by a simple solution route, J. Solid State Chem. 180 (2007) 1390–1396.
[159] Y. Li, B. Tan, Y. Wu, Ammonia-evaporation-induced synthetic method for metal (Cu, Zn, Cd, Ni) hydroxide/oxide nanostructures, Chem. Mater. 20 (2008) 567–576.
[160] L. Bai, F. Yuan, P. Hu, S. Yan, X. Wang, S. Li, A facile route to sea urchin-like NiO architectures, Mater. Lett. 61 (2007) 1698–1700.
[161] D.-F. Zhang, L.-D. Sun, C.-J. Jia, Z.-G. Uan, L.-P. You, C.-H. Yua, Hierarchical assembly of SnO_2 nanorods arrays on α-Fe_2O_3 nanotubes: a case of interfacial lattice compatibility, J. Am. Chem. Soc. 127 (2005) 13492–13493.
[162] Y. Chen, C. Zhu, X. Shi, M. Cao, H. Hin, The synthesis and selective gas sensing characteristics of SnO_2/α-Fe_2O_3 hierarchical nanostructures, Nanotechnology 19 (2008) 205603.
[163] J.Y. Lao, J.G. Wen, Z.F. Ren, Hierarchical ZnO nanostructures, Nano Lett. 2 (2002) 1287–1291.
[164] L. Mazeina, Y.N. Picard, S.M. Prokes, Controlled growth of parallel oriented ZnO nanostructural array on GaO nanowires, Cryst. Growth Des. 9 (2009) 1164–1169.

[165] L. Xu, Y. Su, S. Li, Y. Chen, Q. Zhou, S. Yin, Y. Feng, Self-assembly and hierarchical organization of Ga_2O_3/In_2O_3 nanostructures, J. Phys. Chem. B 111 (2007) 760–766.
[166] C.N.R. Rao, F.L. Deepak, G. Gundiah, A. Govindaraj, Inorganic nanowires, Progr. Solid State Chem. 31 (2003) 5–147.
[167] Y. Xia, P. Yang, Y. Sun, Y. Wu, B. Mayers, B. Gates, Y. Yin, F. Kim, H. Yan, One-dimensional nanostructures: synthesis characterization, and application, Adv. Mater. 15 (2003) 353–389.
[168] Z.R. Dai, Z.W. Pan, Z.L. Wang, Novel nanostructures of functional oxide synthesized by thermal evaporation, Adv. Funct. Mater. 13 (2003) 9–24.
[169] P. Yang, H. Yan, S. Mao, R. Russo, J. Pham, R. He, H.-J. Choi, Controlled growth of ZnO nanowires and their optical properties, Adv. Funct. Mater. 12 (2002) 323–331.
[170] R.-Q. Zhang, Y. Lifshitz, S.-T. Lee, Oxide-assisted growth of semiconducting nanowires, Adv. Mater. 15 (2003) 635–640.
[171] Y. Dai, Y. Zhang, Q.K. Li, C.W. Nan, Synthesis and optical properties of tetrapod-like zinc oxide nanorods, Chem. Phys. Lett. 358 (2002) 83–86.
[172] C.N.R. Rao, G. Gundiah, F.L. Deepak, A. Govindaraj, A.K. Cheetham, Carbon-assisted synthesis of inorganic nanowires, J. Mater. Chem. 14 (2004) 440–450.
[173] H. Uchiyama, H. Ohgi, H. Imai, Selective preparation of SnO_2 and SnO crystals with controlled morphologies in an aqueous solution system, Cryst. Growth Des. 6 (2006) 2186–2190.
[174] Z.R. Dai, Z.W. Pan, Z.L. Wang, Growth and structure evolution of novel tin oxide diskettes, J. Am. Chem. Soc. 124 (2002) 8673–8680.
[175] G. Korotchenkov, V. Mascanov, V. Tolsoty, V. Brinzari, J. Schwank, G. Faglia, Structural and gas response characterization of nano-size SnO_2 films deposited by SILD method, Sens. Actuators B 96 (2003) 602–609.
[176] D.E. Williams, K.F.E. Pratt, Microstructure effects on the response of gas-sensitive resistors based on semiconducting oxides, Sens. Actuators B 70 (2000) 214–221.
[177] G. Korotcenkov, The role of morphology and crystallographic structure of metal oxides in response of conductometric-type gas sensors, Mater. Sci. Eng. R 61 (2008) 1–39.
[178] M. Ivanovskaya, D. Kotsikau, G. Faglia, P. Nelli, Influence of chemical composition and structural factors of Fe_2O_3/In_2O_3 sensors on their selectivity and sensitivity to ethanol, Sens. Actuators B (2003) 498–503.
[179] K.-W. Kim, P.-S. Cho, S.-J. Kim, J.-H. Lee, C.-Y. Kang, J.-S. Kim, S.-J. Yoon, The selective detection of C_2H_5OH using SnO_2–ZnO thin film gas sensors prepared by combinatorial solution deposition, Sens. Actuators B 123 (2007) 318–324.
[180] R. Gutierrez-Osuna, H.T. Nagle, S.S. Schiffman, Transient response analysis of an electronic nose using multi-exponential models, Sens. Actuators B 61 (1999) 170–182.
[181] A. Galdikas, Ž. Kancleris, S. Senulienėm, A. Šetkus, Influence of heterogeneous reaction rate on response kinetics of metal oxide gas sensors: application to the recognition of an odour, Sens. Actuators B 95 (2003) 244–251.
[182] J.-H. Lee, S.-J. Kim, P.-S. Cho, in: R.A. Potyrailo, V.M. Mirsky (Eds.), Combinatorial Methods for Chemical and Biological Sensors, Springer, 2009, pp. 295–312 (Chapter 12).
[183] B.P.J.de.L. Costello, R.J. Ewen, N.M. Ratcliffe, P.S. Sivenand, Thick film organic vapour sensors based on binary mixtures, Sens. Actuators B 92 (2003) 159–166.
[184] J.-Y. Lee, J.-H. Lee, S.-H. Hong, Y.K. Lee, J.-Y. Choi, Uniform coating of nanometer-scale $BaTiO_3$ layer on spherical Ni particles via hydrothermal conversion of Ti-hydroxide, J. Am. Ceram. Soc. 88 (2005) 303–307.
[185] A. Cabot, A. Diéguez, A. Romano-Rodríguez, J.R. Morante, N. Bârsan, Influence of the catalytic introduction procedure on the nano-SnO_2 gas sensor performances, where and how stay the catalytic atoms, Sens. Actuators B 79 (2001) 98–106.
[186] Y. Shimizu, N. Matsunaga, T. Hyodo, M. Egashira, Improvement of SO_2 sensing properties of WO_3 by noble metal loading, Sens. Actuators B 77 (2001) 35–40.
[187] M. Yuasa, T. Masaki, T. Kida, K. Shimanoe, N. Yamazoe, Nano-sized PdO loaded SnO_2 nanoparticle by reverse micelle method for highly sensitive CO gas sensor, Sens. Actuators B 136 (2009) 99–104.
[188] Y.C. Lee, H. Huang, O.K. Tan, M.S. Te, Semiconductor gas sensor based on Pd-doped SnO_2 nanorod thin films, Sens. Actuators B 132 (2008) 239–242.
[189] N.V. Hieu, H.-R. Kim, B.-K. Ju, J.-H. Lee, Enhanced performance of SnO_2 nanowires ethanol sensor by functionalizing with La_2O_3, Sens. Actuators B 133 (2008) 228–234.
[190] U.-S. Choi, G. Sakai, N. Yamazoe, Sensing properties of Au-loaded SnO_2–Co_3O_4 composites to CO and H_2, Sens. Actuators B 107 (2005) 397–401.
[191] J. Tamaki, K. Shimanoe, Y. Yamada, Y. Yamamoto, N. Miura, N. Yamazoe, Dilute hydrogen sulfide sensing properties of CuO–SnO_2 thin film prepared by low-pressure evaporation method, Sens. Actuators B 49 (1998) 121–125.
[192] W. Shen, Y. Zhao, C. Zhang, The preparation of ZnO based gas-sensing thin films by ink-jet printing method, Thin Solid Films 483 (2005) 382–387.

Biography

Jong-Heun Lee has been a Professor at Korea University since 2008. He received his BS, MS, and PhD degrees from Seoul National University in 1987, 1989, and 1993, respectively. Between 1993 and 1999, he developed automotive air-fuel-ratio sensors at the Samsung Advanced Institute of Technology. He was a Science and Technology Agency of Japan (STA) fellow at the National Institute for Research in Inorganic Materials (currently NIMS, Tsukuba, Japan) from 1999 to 2000, a research professor at Seoul National University from 2000 to 2003, and an associate professor at Korea University from 2003 to 2008. His current research interests include chemical sensors, functional nanostructures, and solid oxide electrolytes.